Journal of Advanced Research 61 (2024) 65–81

Contents lists available at ScienceDirect

Journal of Advanced Research

journal homepage: www.elsevier.com/locate/jare

Triad3A-Mediated K48-Linked ubiquitination and degradation of TLR9 impairs mitochondrial bioenergetics and exacerbates diabetic cardiomyopathy

Chunyan Kong [a,b,1], Zhen Guo [a,b,1], Fangyuan Liu [a,b,1], Nan Tang [a,b], Mingyu Wang [a,b], Dan Yang [a,b], Chenfei Li [a,b], Zheng Yang [a,b], Yulan Ma [a,b], Pan Wang [a,b], Qizhu Tang [a,b,*]

[a] Department of Cardiology, Renmin Hospital of Wuhan University, Wuhan 430060, PR China
[b] Hubei Key Laboratory of Metabolic and Chronic Diseases, Wuhan, PR China

HIGHLIGHTS

- Cardiac-specific TLR9 overexpression in diabetic mice relieved cardiac dysfunction, and remodeling.
- TLR9 modulated energy metabolism in diabetes heart, but not canonical inflammatory signaling.
- Triad3A can interact with TLR9 and promote its proteasomal degradation by catalyzing K48-linked ubiquitination.
- PGC-1 and AMPK mediated TLR9's defense against diabetic cardiac damage and dysfunction.

GRAPHICAL ABSTRACT

Triad3A elevation induced by STZ or HG stimulation leads to degradation of TLR9 K48-linked proteasomal ubiquitination, which impairs mitochondrial function and reduces the AMP/ATP ratio and inhibits the activation of AMPK and PGC-1, which in turn leads to oxidative stress, apoptosis and fibrosis and other pathological changes. STZ: Streptozotocin; HG: High glucose; TLR9: Toll-like receptor 9; AMP: Adenosine monophosphate; ATP: Adenosine triphosphate; AMPK: Adenosine 5'-monophosphate (AMP)-activated protein kinase; PGC-1α: Peroxisome-proliferator-activated receptorγcoactivator-1α.

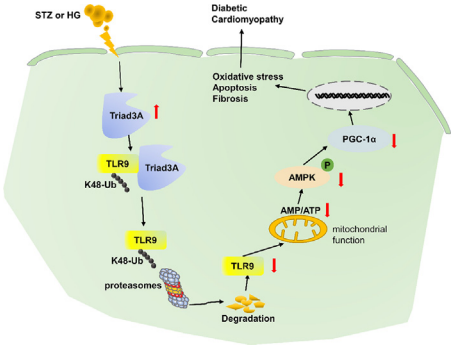

ARTICLE INFO

Article history:
Received 23 April 2023
Revised 2 August 2023
Accepted 21 August 2023
Available online 23 August 2023

ABSTRACT

Introduction: Targeted protein degradation represents a promising therapeutic approach, while diabetic cardiomyopathy (DCM) arises as a consequence of aberrant insulin secretion and impaired glucose and lipid metabolism in the heart..

Objectives: Considering that the Toll-like receptor 9 (TLR9) signaling pathway plays a pivotal role in regulating energy metabolism, safeguarding cardiomyocytes, and influencing glucose uptake, the primary

Abbreviations: DM, Diabetes mellitus; DCM, diabetic cardiomyopathy; TLR9, Toll-like receptor 9; CPG, Cytosine Phosphate Guanine; HFD, high-fat diet; TAC, transverse aortic constriction; AAV9, Adeno-associated virus serotype 9; STZ, streptozotocin; NRCMs, neonatal rat cardiomyocytes; FBS, fetal bovine serum; AMCMs, adult mouse cardiomyocytes; TUNEL, terminal deoxynucleotidyl transferase dUTP nick-end labeling; DAB, diaminobenzidine; ECAR, extracellular acidification rates; OCR, oxygen consumption rate; DHE, Dihydroethidium; IP, Immunoprecipitation; GST, Glutathione S-Transferase; HPLC, high-performance liquid chromatography; ATP, adenosine triphosphate; ADP, adenosine diphosphate; AMP, adenosine monophosphate; MDA, malondialdehyde; 4-HNE, 4 hydroxynonenal; LVEF, left ventricular ejection fraction; LVFS, left ventricular fractional shortening; CO, cardiac output; LVIDd, left ventricular diastolic diameter; AMPK, AMP-activated kinase.

* Corresponding author at: Department of Cardiology, Renmin Hospital of Wuhan University, Cardiovascular Research Institute, Hubei Key Laboratory of Metabolic and Chronic Diseases, Wuhan University at Jiefang Road 238, Wuhan 430060, PR China.
E-mail address: qztang@whu.edu.cn (Q. Tang).
[1] These authors have contributed equally to this work.

https://doi.org/10.1016/j.jare.2023.08.015

Keywords:
Diabetic cardiomyopathy
Toll-like receptor 9
Triad3A
Ubiquitination
Mitochondrial bioenergetics

objective of this study was to investigate the impact of TLR9 on diabetic cardiomyopathy (DCM) and elucidate its underlying mechanism.
Methods: Mouse model of DCM was established using intraperitoneal injection of STZ, and mice were transfected with adeno-associated virus serotype 9-TLR9 (AAV9-TLR9) to assess the role of TLR9 in DCM. To explore the mechanism of TLR9 in regulating DCM disease progression, we conducted interactome analysis and employed multiple molecular approaches.
Results: Our study revealed a significant correlation between TLR9 expression and mouse DCM. TLR9 overexpression markedly mitigated cardiac dysfunction, myocardial fibrosis, oxidative stress, and apoptosis in DCM, while inflammation levels remained relatively unaffected. Mechanistically, TLR9 overexpression positively modulated mitochondrial bioenergetics and activated the AMPK-PGC1a signaling pathway. Furthermore, we identified Triad3A as an interacting protein that facilitated TLR9′s proteasomal degradation through K48-linked ubiquitination. Inhibiting Triad3A expression improved cardiac function and pathological changes in DCM by enhancing TLR9 activity.
Conclusions: The findings of this study highlight the critical role of TLR9 in maintaining cardiac function and mitigating pathological alterations in diabetic cardiomyopathy. Triad3A-mediated regulation of TLR9 expression and function has significant implications for understanding the pathogenesis of DCM. Targeting TLR9 and its interactions with Triad3A may hold promise for the development of novel therapeutic strategies for diabetic cardiomyopathy. Further research is warranted to fully explore the therapeutic potential of TLR9 modulation in the context of cardiovascular diseases.

Introduction

Diabetes mellitus (DM) represents a global health challenge, with cardiovascular complications being the leading cause of morbidity and mortality in diabetic individuals. DM exerts detrimental effects on the cardiovascular system, particularly the heart, through various pathological mechanisms, including alterations in energy metabolism, mitochondrial dysfunction, and oxidative stress [1]. These mechanisms ultimately lead to structural and functional abnormalities in the myocardium, contributing to the development of diabetic cardiomyopathy (DCM) [2,3]. However, the research and understanding of DCM are currently not well-elaborated, and clinical drug treatments for DCM remain largely nonspecific.

Recent investigations have implicated Toll-like receptor 9 (TLR9) in the pathogenesis of metabolic-related cardiovascular disorders. While primarily expressed in immune cells [4], TLR9 has also been detected in non-immune cells like cardiac myocytes [5]. TLR9 negatively regulates the development of islets and insulin-secreting cells in type 1 diabetes, offering new avenues for designing prevention or treatment strategies for diabetes [6]. Furthermore, β-cell TLR9 has been found to play a pivotal role in immune tolerance to islet β-cell autoimmunity, as β-cell TLR9 deficiency strongly protects NOD mice from the pathogenesis of T1D [7]. In the context of cardiomyocytes, TLR9 activation mediated by Cytosine Phosphate Guanine (CPG) oligonucleotide (CPG-ODN) has demonstrated cardioprotective effects against pathological ischemia by regulating energy metabolism, as observed in both in vitro and in vivo experiments [8,9]. Additionally, CpG treatment has been shown to reduce apoptosis and cardiomyocyte loss, alleviate myocardial remodeling and scar area, and lead to significantly improved LV function [10]. While TLR9 enhances the proliferation and differentiation of myocardial fibroblasts, resulting in considerable improvement in cardiac rupture, it does not seem to participate in the acute response, as noted by Omiya et al [11]. Furthermore, TLR9-KO mice stimulated by a high-fat diet (HFD) exhibit increased insulin resistance and amplified metabolic disorders caused by HFD [12]. Moreover, Liu et al. found that TLR9 deletion resulted in impaired glucose uptake by skeletal muscle in mice, leading to decreased blood glucose levels [13]. These findings indicate a close association between TLR9 and the onset and progression of metabolic cardiovascular diseases.

Triad3A, an E3 ubiquitin-protein ligase, plays a critical role in the ubiquitination and proteolytic degradation of specific Toll-like receptors (TLRs) [14]. Through this ubiquitination process, Triad3A regulates the intensity and duration of TLR signaling [14,15]. Notably, Triad3A interacts with the TIR domain in the cytoplasmic tails of various TLRs, including TLR3, TLR4, TLR5, and TLR9, with particularly high binding affinity for TLR4 and TLR9 [14,16]. Triad3A shows promise as a candidate in cardiac disease research, particularly in the context of cardiomyopathy. Prior studies have shown that elevated Triad3A expression mitigates transverse aortic constriction (TAC)-induced cardiac hypertrophy by inducing polyubiquitination and degradation of TLR4 and TLR9, which leads to the inhibition of NF-κB and AKT signaling [16]. In addition, this study also found that Triad3A is mainly expressed in cardiomyocytes [16], it can be expressed in inflammatory cell-infiltrated cardiomyocytes and cardiac fibroblasts, and is altered in the progression of cardiac hypertrophy [51,52]. However, the precise role and mechanism of Triad3A in diabetic cardiomyopathy remain poorly understood.

Considering the metabolic alterations observed in DCM, there might be a distinctive interplay between DCM and the biology of TLR9. However, the specific effects and underlying mechanisms of TLR9 in DCM have not been fully elucidated. In this study, we found that TLR9 expression was downregulated in the myocardial tissues of DCM mice and high-glucose stimulated cardiomyocytes. Notably, TLR9 overexpression ameliorated cardiac dysfunction, myocardial remodeling, oxidative stress, apoptosis, and energy metabolism in DCM, while exerting no significant effect on inflammatory responses and signaling pathways. Mechanistically, we uncovered that Triad3A-mediated degradation of TLR9 ubiquitination exacerbates diabetic cardiomyopathy in mice through the AMPKα/PGC-1α pathway. Consequently, Triad3A and TLR9 emerge as promising therapeutic targets for addressing DCM.

Materials and methods

Animals studies

All animal experiments were performed in accordance with the Guidelines for the Care and Use of Laboratory Animals (NIH publication, revised 2011) and approved by the Animal Care and Use

Committee of Renmin Hospital of Wuhan University (IACUC Issue No. WDRM20171201). Adult Male TLR9KO mice (C57BL/6 background, The Jackson Laboratory; 8–10 weeks old; 23.5–27.5 g) and WT C57BL/6 mice (8–10 weeks old; 23.5–27.5 g) were purchased from the Institute of Laboratory Animal Science, Chinese Academy of Medical Sciences (Beijing, China). The source of AMPKα2 global knockout mice and PGC-1α cardiac specific-knockout mice has been described previously [17,18]. The animals were housed in a pathogen-free setting with ideal temperature and humidity.

Adeno-associated virus serotype 9 (AAV9) vectors carrying the TLR9 (AAV9-TLR9) gene under a cTnT promoter or negative control (AAV9-VEC), AAV9 carrying small hairpin RNA (shRNA) against Triad3A (AAV9-shTriad3A) or a correspondingly negative control AAV9-shRNA were generated by DesignGene Biotechnology (Shanghai, China). Mice were anesthetized by intraperitoneal injection of pentobarbital (50 mg/kg) followed by in situ injection of virus solution (1×10^{11} vp (viral particles) per animal) at multiple points on the myocardial surface. Four weeks after the AAV9 injection, the animals were randomly assigned to either a vehicle treatment or STZ treatment. Treatment and follow-up analysis were performed by blind method.

Mice were rendered diabetic by administering streptozotocin (STZ, Sigma, St. Louis, MO) intraperitoneally five days in a row at a dose of 50 mg/kg dissolved in a 100 mM citrate buffer at pH 4.5. This was done to imitate cardiac injury in type 1 diabetes. An identical amount of citrate buffer was administered to the mice in the vehicle control group. Starting on day 3, glucometer measurements of fasting blood glucose levels were made. Mice with fasting glucose levels > 16.7 mmol/l for three days in a row were deemed diabetic. Body weights and fasting glucose levels of all mice were monitored weekly throughout the study. The remaining mice were sacrificed 16 weeks after the onset of diabetes.

One day before the sacrifice, transthoracic echocardiography was used to noninvasively monitor the systolic and diastolic heart function in anesthetized mice. Mice were anesthetized by inhalation of 1.5% isoflurane followed by high-frequency, high-resolution echocardiography (Vevo®3100 VisualSonics, Toronto, Canada). Blood samples were collected during euthanasia under anesthesia with an overdose of sodium pentobarbital (200 mg/kg, ip) for further analysis. For the pathological study, heart tissue was taken, fixed in 4% paraformaldehyde, and/or quickly frozen in liquid nitrogen for studies of gene and protein expression.

Cell culture and treatments

The primary neonatal rat cardiomyocytes (NRCMs) were extracted from 3-day-old Sprague-Dawley rats and cultivated in normal medium with 10% fetal bovine serum (FBS) at 37 °C in an incubator gassed with 5% carbon dioxide for the in vitro investigations [18]. After synchronization in serum-free medium for 12 h, Cardiomyocytes were exposed to 33 mM glucose to study the effects of high glucose levels. To overexpress TLR9, adenoviruses were utilized at a multiplicity of infection (MOI) of 50 for 24 h. For inhibition of AMPKα or PGC-1α, NRCMs were incubated with AMPK inhibitor Dorsomorphin (Dors, 10 μM, HY13418A, MCE) or PGC-1α inhibitor SR-18292 [19] (10 μM; HY-101491, MCE).

As previously described [20], adult mouse cardiomyocytes (AMCMs) were harvested. An aseptic procedure was used to remove the heart, which was then placed in a Ca^{2+}-free Tyrode's solution at 4 °C before being pre-cooled and hung in a Langendorff isolated cardiac perfusion system. Aortic cannulation was followed by reversal of the aorta and Tyrode's solution promotion by 95% O_2 + 5% CO_2. The excised heart was first submerged and perfused in Ca^{2+}-free Tyrode's solution for three minutes, followed by an enzymatic digestion solution (type II collagenase, 1.5 g/L), which caused the heart to expand and soften. To get cardiomyocytes, the ventricle was sliced, digested, filtered, centrifuged, suspended, and divided into tissue pieces of 1–2 mm^3.

Cardiomyocytes taken from adult TLR9KO and WT mice [21] were transfected with siTriad3A (50 nmol/L) using LipofectamineTM 6000 for 4 h, and then cultured in normal medium for a further 24 h before being treated with HG, to ascertain the involvement of Triad3A [22].

Histology and tissue staining

Heart tissues collected from all studied groups were fixed with 10% neutral formalin buffer overnight, embedded with paraffin and sectioned at 5 μm thickness. PSR staining was performed to evaluate cardiac fibrosis. The stained sections were observed and photographed using a light microscope and a Nikon photoimaging System (Tokyo, Japan) at a magnification of 200 ×. Paraffin sections were also used to perform terminal deoxynucleotidyl transferase dUTP nick-end labeling (TUNEL) staining for cardiac cell death using ApopTag Plus in Situ Apoptofluorescein Detection kit (Millipore, MIT, USA), the lesions were observed and photographed under the OLYMPUS DX51 fluorescence microscope and analyzed using digital analysis software (Image-Pro Plus 6.0).

Paraffin sections were also used to perform immunohistochemistry for TLR9 (Santa cruz, sc-25468), 4-hydroxynonenal (ABCAM, ab46545) anti-CD45 (ABCAM, ab10558), anti-CD68(ABCAM, ab125212), and anti-PGC-1α (ABCAM, ab54481) using routine techniques. Immunoreactivity was detected by diaminobenzidine (DAB).

Transmission electron microscopy

As previously reported [23], transmission electron microscopy analysis was employed to access the mitochondrial damage in the heart. Heart fragments measuring 1 mm^3 from the left ventricular wall were frozen in 1.25% glutaraldehyde for an entire night at 4 °C (v:v in 0.1 M sodium cacodylate, pH 7.2). Thin sections of the heart samples were photographed on a Tecnai-20 electron microscope (Philips-FEI, Hillsboro, Oregon) after being post-fixed and rinsed three times in 0.1 M sodium cacodylate for 30 min.

Seahorse extracellular flux analyzer assays

A Seahorse XFe24 extracellular flux analyzer was used to assess AMCMs and mitochondrial bioenergetics in intact caSMC and caEC. According to the manufacturer's instructions [23], we carried out glycolysis stress tests and energy substrate (glucose and palmitate) oxidation using mitochondria stress testing. Dose-titration assays were used to establish the oligomycin-A and FCCP working concentrations needed for caSMC and caEC, respectively, in mitochondria stress tests. In V-7 Seahorse plates, 20,000 caSMC and 25,000 caEC per well were grown.

Prior to the assay, AMCMs were cultured in glucose-free Seahorse assay media with 1 mM pyruvate for 1 h at 37 °C in an incubator without CO_2 Glycolysis, glycolytic capacity, and glycolytic reserves were calculated as extracellular acidification rates (ECAR) after injectors were loaded with 20 mM glucose, 1 μM oligomycin, and 100 mM 2-DG.

AMCMs were cultured for 1 h before to the experiment in glucose-free Seahorse assay media supplemented with 1 mM pyruvate at 37 °C in an incubator without CO_2. During a mitochondria stress test, injectors were loaded to add 20 mM glucose, 1 μM Oligomycin, 1 μM FCCP, 1 μM Rotenone, and 2 μM Antimycin A. The oxygen consumption rate (OCR) was determined using exogenous glucose oxidation together with other mitochondria stress test characteristics as basal respiration, maximal respiration, spare

capacity, ATP production, proton leak, and non-mitochondrial respiration.

Immunofluorescence analysis

For immunofluorescence staining in vivo, paraffin-embedded sections of mouse heart tissue were incubated with primary mouse antibodies directed against Nrf2, and α-actin in a humidified chamber at 4 °C overnight. The sections were subsequently incubated with anti-mouse and anti-rabbit secondary antibodies for 1 h in the dark. TLR9 localization in NRCMs was determined by immunofluorescence staining. Briefly, cells were subsequently fixed with 3.7% formaldehyde, permeabilized with 0.1% Triton X-100 in PBS for 45 min, and stained with TLR9 (Santa cruz, sc-25468), followed by the incubation with Alexa Fluor®568-conjugated secondary antibodies at 37℃ for 1 h. Finally, the cell nuclei were probed by DAPI and the fluorescence images were recorded by a fluorescence microscope in a blinded manner.

Intracellular ROS Detection

Intracellular ROS levels were evaluated through dihydroethidium (DHE) staining. Briefly, fresh heart samples were sectioned and incubated with DHE (1 μM) for 30 min. For DHE staining of NRCMs, cells were incubated with DMEM/F12 (C11995500BT, GIBCO) containing 5 μM DHE at 37 °C for 30 min to load the fluorescent probe, then washed with PBS three times and observed directly under the microscope.

Immunoblotting and real-time PCR

RIPA lysis buffer was used to lyse left ventricular tissues and cultured cardiomyocytes, and protein content was measured using a BCA protein assay kit (Thermo Scientific, 23227). SDS-PAGE was used to separate the lysates, which were then electro-transferred onto PVDF membranes. Before incubation with the primary antibodies, the membranes were blocked for 1 h at room temperature with 5% skimmed milk diluted in Tris-buffer saline with Tween-20 (TBST). The membranes were then incubated overnight at 4 °C with the primary antibodies, followed by incubation with a matching secondary antibody. Bio-Rad ChemiDocTM XRS was used to view the bands (Bio-Rad). **Supplementary Table 1** lists the principal antibodies utilized.

RNA extraction and reverse transcriptase-polymerase chain reaction (Transcriptor First Strand cDNA Synthesis Kit, Roche, Basel, Switzerland) were used to determine mRNA expression. The PCR reaction was carried out using the LightCycler 480 SYBR Green Master Mix, and the PCR product amount was normalized to GAPDH. For quantitative gene expression analysis, the $2^{-\Delta\Delta CT}$ approach was applied. **Supplementary Table 2** lists the primers that were utilized.

Plasmid construction and transfection

Plasmids harboring full-length human and full-length rat Triad3A were cloned into Flag vector. Ubiquitin was cloned into the flag vector. Full-length human TLR9 and lysine-site-mutated human TLR9 were cloned into the Myc GV219 vector. The following mutant Ub plasmids were created: K6O, K11O, K27O, K48O, K63O, and K48R. **Supplementary Table 3** lists the primer sequences utilized in the creation of plasmids.

Immunoprecipitation (IP) assays and Glutathione s-transferase (GST) precipitation assays

IP assays were performed as described previously [24]. Transfected NRCMs or Hearts tissues were lysed with IP lysis buffer. For co-immunoprecipitation (co-IP) assays, HEK293T cells were co-transfected with indicated plasmids and then lysed with cold IP buffer. Samples were lysed on ice for 10 min and centrifuged at 12,000 g for 10 min. The 500 μl supernatants were incubated with 20 μl protein A/Gagarose beads (Calbiochem #IP05) and 1μg corresponding antibody at 4 °C for 3 h. Then the beads were washed with cold IP buffer three times and boiled with 1 × SDS loading buffer before Western blotting analysis.

For the GST pull-down assay, HEK293T cells were collected and lysed using lysis buffer (50 mM Na2HPO4, pH 8.0; 300 mM NaCl; 1 % Triton X-100; Protease Inhibitor Cocktail (04693132001, Roche, Basel, Switzerland), 24 h after transfected with GST-TLR9 plasmid or HA-Triad3A plasmid. After centrifugation at 4 °C, GST-TLR9 proteins were purified with Glutathione Sepharose 4B beads (#17075601, GE Healthcare) for 3 h and then incubated with purified HA-Triad3A proteins overnight at 4 °C. The beads were then rinsed with washing buffer and denatured for 10 min at 95 °C with 2 SDS loading buffer before being analyzed with Western blotting.

Ubiquitination assays

Cultured NRCMs or heart tissues were lysed in SDS lysis buffer (20 mM Tris–HCl, pH 7.4, 150 mM NaCl, 1 mM EDTA, 1 % SDS) including protease inhibitor cocktail (04693132001, Roche, Basel, Switzerland). After denaturation by heating at 95 °C for 10 min, the lysates were diluted 10-fold with IP buffer (20 mM Tris10 HCl pH 7.4, 150 mM NaCl, 1 mM EDTA, and 1 %Triton X-100). The lysates were then centrifuged at 15,000 rpm for 10 min at 4 °C before being submitted to IP tests with the specified antibodies, followed by western blot.

AMP, ADP, and ATP measurements

Frozen LVs and collected CMs were transferred to ice-cold 0.6 M $HClO_4$ (4 mL/g), and the tissue or NRCMs was immediately homogenized and centrifuged (10 000g, 4 °C, 10 min). After being neutralized with an equivalent amount of 1 M Na_2HPO_4, the supernatant was centrifuged once more at 10,000g and 4 °C for ten minutes. Using a 0.22 m filter, the supernatant was filtered. A Beckman C18 column (5 m, 250 4.6 mm) was used for the high-performance liquid chromatography (HPLC) technique to evaluate 50 μl aliquots. Analytes were isocratically eluted using 96% 0.05 M KH_2PO_4 (pH 6.5) and 4% methanol for 30 min. An external standard approach was used to quantify adenosine triphosphate (ATP), adenosine diphosphate (ADP), and adenosine monophosphate (AMP) concentrations at 254 nm.

Determination of lipid Peroxidation, SOD activity

To further assess oxidative stress level, myocardial malondialdehyde (MDA) or 4 hydroxynonenal levels (4-HNE) level, SOD activities in the myocardial tissues were determined using commercially available kits procured from Beyotime Co. (Nantong, China) according to a previous study [25].

Statistical analysis

Individual data points are shown in Figures, and results are reported as mean ± SEM from at least three different experiments. The unpaired student *t*-test or one-way ANOVA followed by the Tukey post hoc test was used to determine the statistical signifi-

cance of differences between groups. Differences were considered to be significant at $p < 0.05$. GraphPad Prism (version 8.0, GraphPad Software, San Diego, CA) and IBM SPSS Statistics 22.0 (IBM Corporation) were used for statistical analysis [26,27]. In the Figures, each point represents a biological replicate and, if no other indication is made.

Results

Diminished TLR9 expression in HG-Treated NRCMs and diabetic mice heart

We initiated our study by examining changes in TLR9 expression levels in HG stimulated NRCMs to investigate its potential role in diabetic cardiomyopathy. Western blot analysis revealed a time-dependent down-regulation of TLR9 protein levels under HG stimulation, with the most significant reduction observed after 24 h (Fig. 1**A**). Immunofluorescence labeling further confirmed a considerable decrease in TLR9 expression in HG-stimulated cardiomyocytes (Fig. 1**B**).

To establish the diabetic cardiomyopathy model, we monitored blood glucose levels, cardiac function, and performed HE staining of cardiac tissue in STZ-induced mice over 16 weeks (**Fig. S1A–S1D**). Additionally, we assessed TLR9 expression levels in the heart tissues of these diabetic mice models, which showed a significant reduction in TLR9 protein levels compared to control hearts (Fig. 1**C**). Immunohistochemical staining further confirmed decreased TLR9 expression in the hearts of mice with diabetic cardiomyopathy compared to control mice (Fig. 1**D**). It is strongly advised that TLR9 be engaged in DCM given the decline in TLR9 protein level.

TLR9 overexpression attenuates Diabetes-Induced cardiac dysfunction and remodeling

Mice transfected with AAV9-TLR9 were utilized to investigate the direct association between TLR9 overexpression and DCM.

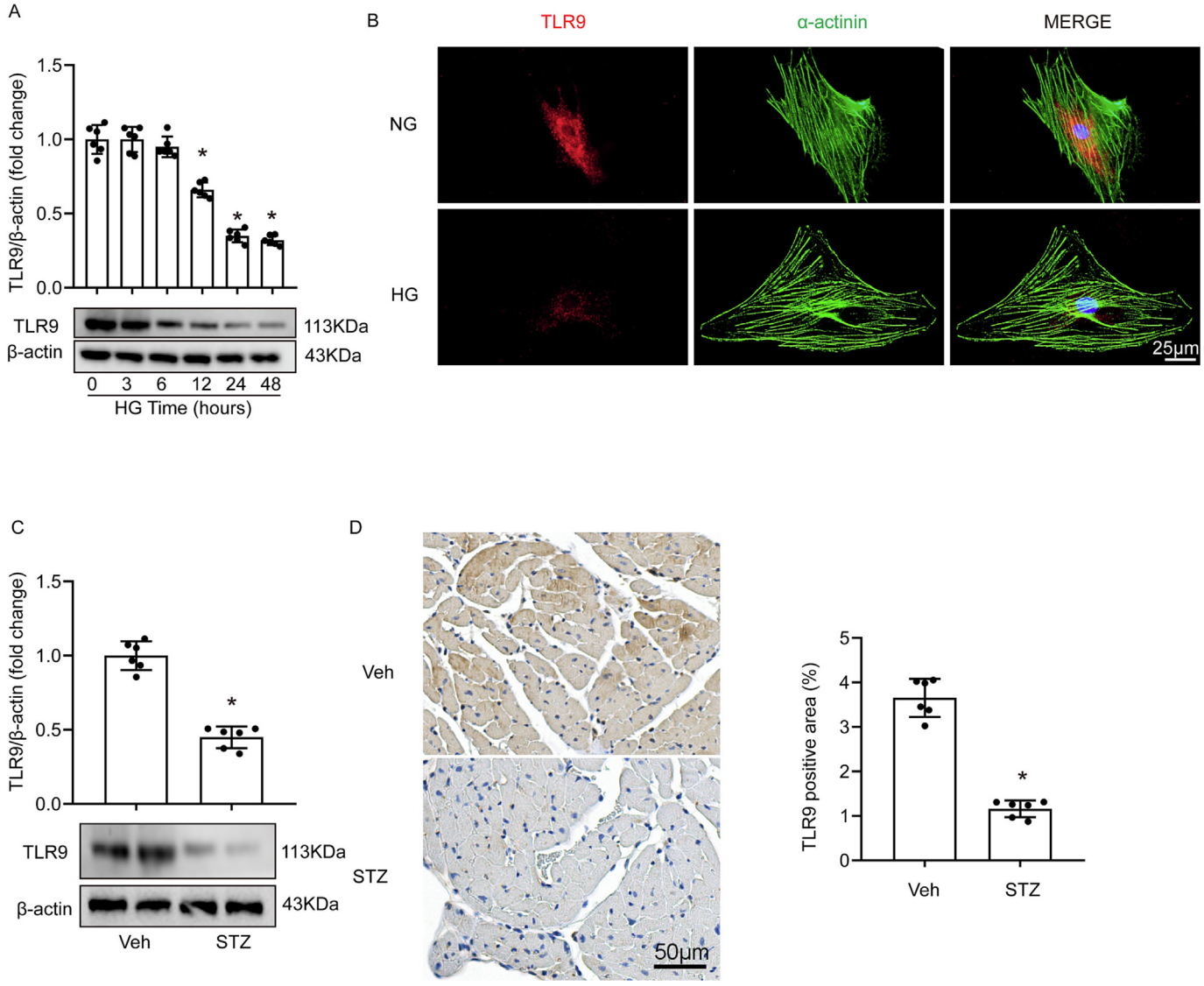

Fig. 1. Decreased TLR9 levels in HG-stimulated cardiomyocytes and diabetic mice heart. A. TLR9 level in NRCMs stimulated by high glucose (HG) at different time periods (n = 6); *$p < 0.05$ vs the PBS group; B. Representative images of immunofluorescence of TLR9 (red), and α-actinin (green) in HG-treated NRCMs (n = 6); C. Representative western blot analysis of TLR9 in cardiac tissues from healthy and diabetic mice (n = 6); D. Immunohistochemical staining of TLR9 in heart tissues from healthy and diabetic mice (n = 6). *$p < 0.05$ vs the Veh group. (For interpretation of the references to colour in this figure legend, the reader is referred to the web version of this article.)

AAV9-TLR9 #1 markedly increased the level of TLR9 protein in NRCMs (**Fig. S2A**). When compared to the AAV-VEC transduced group, **Fig. S2B** demonstrates that the TLR9 levels in the myocardium were much higher following AAV9-TLR9 transduction. The presence of hyperglycemia was demonstrated in AAV9-VEC (AAV9-VEC + STZ) and AAV9-TLR9 diabetic mice (AAV9-TLR9 + STZ) for up to 16 weeks. Overexpression of TLR9 had no discernible effects on fasting blood sugar levels. (Fig. 2**A**).

Hemodynamic analysis using the Millar transducer revealed that AAV9-TLR9 + STZ mice exhibited increased peak derivative of pressure over time (+dP/dt max) and decreased peak derivative of pressure over time (-dP/dt min) compared to AAV9-VEC + STZ mice (Fig. 2**B-2C**). Furthermore, TLR9-overexpressing mice demonstrated significantly improved cardiac systolic function relative to STZ-treated WT mice, as indicated by increased left ventricular ejection fraction (LVEF), left ventricular fractional shortening (LVFS), cardiac output (CO), and decreased left ventricular diastolic diameter (LVIDd) (Fig. 2**D-2H**). TLR9 overexpression also ameliorated diastolic dysfunction in diabetic mice, as evidenced by the early mitral diastolic waves/mitral raised late diastolic wave ratio (E/A ratio), determined by pulsed Doppler study of mitral blood flow patterns (Fig. 2**I**).

Cardiac fibrosis was assessed using Sirius Red staining of mouse heart tissues. PSR labeling revealed significant heart fibrosis in diabetic animals, which was protected by TLR9 overexpression (Fig. 2**-J-2 K**). Western blot analysis of diabetic mouse hearts showed increased expression of col1 and α-SMA, which were markedly down-regulated following AAV9-TLR9 injection (Fig. 2**L-2 N**). Moreover, TLR9 overexpression substantially reduced the mRNA expression of cardiac fibrosis indicators, including connective tissue growth factor (ctgf), col1, and collagen III (col III) (Fig. 2**O**). These findings imply that in diabetic mice, TLR9 attenuates cardiac dysfunction and myocardial remodeling.

TLR9 protected mice hearts from oxidative damage and cardiomyocytes apoptosis in diabetic context

The pathogenesis of DCM is facilitated by elevated oxidative stress and apoptosis. To assess ROS levels in cardiac tissues, DHE probes were employed. The results revealed significantly higher DHE fluorescence intensities in the cardiac tissues of diabetic mice compared to mice treated with vehicle, which were attenuated by TLR9 overexpression (Fig. 3**A**). AAV9-TLR9 treatment also led to a reduction in the elevated levels of 3-NT, MDA, and 4-HNE, and a decrease in SOD activity in the heart tissues of diabetic mice (Fig. 3**B-3F**). Immunohistochemical examination of cardiac 4-HNE further confirmed that lipid peroxidation was reduced in the AAV9-TLR9 + STZ group compared to the AAV9-VEC + STZ group (Fig. 3**G-3H**). Western blot analysis revealed that TLR9 significantly upregulated SOD2 expression and downregulated the NADPH oxidase subunit P67phox in the hearts of diabetic mice (Fig. 3**I-3 K**).

TLR9 reduced the number of TUNEL-positive nuclei observed in cardiac tissues following STZ injection, as demonstrated by TUNEL staining (Fig. 3**L-3 M**). Western blot analysis further supported the inhibitory effects of TLR9 on cardiomyocyte apoptosis by showing that TLR9 upregulated BCL-2 and downregulated BAX levels (Fig. 3**-N-3P**).

TLR9 modulated mitochondrial bioenergetics in diabetes Heart, but not canonical inflammatory signaling

It has been revealed that, in addition to the traditional TLR9 inflammatory signaling pathway, controlling energy metabolism also confers protection to cardiomyocytes and neurons [28]. High-resolution electron microscopy analysis of mitochondrial morphology demonstrated severe damage in diabetic cardiac tissues, including inflation, decreased number of mitochondrial cristae, absence of cristae, and irregularities. However, TLR9 overexpression significantly ameliorated mitochondrial damage in diabetic mice (Fig. 4**A-4E**). To assess the impact of TLR9 on mitochondrial function, key enzymes related to mitochondrial function were measured. TLR9 overexpression resulted in enhanced pyruvate dehydrogenase activity and citrate synthase in the diabetic hearts (Fig. 4**F-4G**). Moreover, mitochondrial oxidative phosphorylation and glycolysis rates were evaluated in mouse AMCMs based on the OCR and ECAR rates. TLR9 overexpression in T1DM hearts clearly increased mitochondrial respiratory capacity (Fig. 4**H**). Additionally, in AMCMs derived from T1DM mice, TLR9 boosted glycolytic capacity and mildly increased basic glycolysis (Fig. 4**I**). Subsequently, heart energy metabolism was measured, and it was found that TLR9 overexpression dramatically elevated the levels of ATP, AMP, and ADP, as well as the ratios of AMP/ATP and ADP/ATP compared with diabetic hearts administered with AAV9-VEC and AAV9-TLR9 (Fig. 4**J-4 N**). These results indicate that TLR9 restores mitochondrial activity and positively influences the bioenergetics of mitochondria.

In the hearts of diabetic mice, there was a significant increase in the infiltration of CD45-labeled leukocytes and CD68-labeled macrophages. Contrary to expectations, TLR9 overexpression had no discernible impact on myocardial tissue inflammation in diabetic heart disease, neither exacerbating nor reducing the inflammatory response in the hearts of STZ-induced diabetic mice (**Fig. S3A-S3C**). The mechanism of TLR signaling has been the subject of previous investigations, which have demonstrated that TLR signaling involves the recruitment of various linker molecules that activate NF-κB pathways, thus expediting the inflammatory response [29]. However, we discovered that overexpressing TLR9 did not affect IκBα phosphorylation and subsequent degradation in myocardial tissue, nor did it affect canonical NF-κB P65 activation and nuclear translocation, or the elevation of Myd88 expression induced by STZ (**Fig. S3D-S3H**). These findings suggest that TLR9 plays a role in controlling energy metabolism in diabetic cardiomyopathy but does not significantly influence inflammatory reactions or conventional inflammatory pathways.

TLR9 contributes to the PGC-1α activation and Nrf2 activation and nuclear translocation

The activation of AMP-activated kinase (AMPK) is primarily triggered by an increase in the AMP/ATP ratio [30,31]. AMPK activation enhances cellular tolerance to metabolic stress by inhibiting ATP-depleting pathways that are not essential for short-term cell survival [32]. TLR9 upregulated AMPKα2 phosphorylation in the cardiac tissues of diabetic mice (Fig. 5**A-5B**). PGC-1α is involved in glucose uptake, gluconeogenesis, insulin secretion, and mitochondrial biogenesis [33]. PGC-1α is thought to mediate AMPK-induced gene expression. Activation of AMPK leads to increased expression of PGC-1α [34], and AMPK requires PGC-1α activity to regulate several key aspects of mitochondrial and glucose metabolism [35]. We next investigated the specific mechanisms related to energy metabolism through which TLR9 protects against diabetes-related heart damage. Western blots showed that TLR9 significantly preserved PGC-1α expression in STZ-treated mouse hearts (Fig. 5**A–5C**). Immunohistochemistry results demonstrated that STZ decreased PGC-1α levels, while TLR9 partially increased PGC-1α expression in diabetic hearts (Fig. 5**I–5J**). To further clarify how TLR9 reduces oxidative stress, we investigated the Nrf2/HO-1 pathway. Nrf2 plays a significant protective role in the oxidative stress response and peroxide production during diabetes [36,37]. We found that TLR9 increased the levels of Nrf2 and HO-1 in diabetic hearts and may be responsible for Nrf2′s nuclear translocation, as evidenced by western blots of nuclear protein and

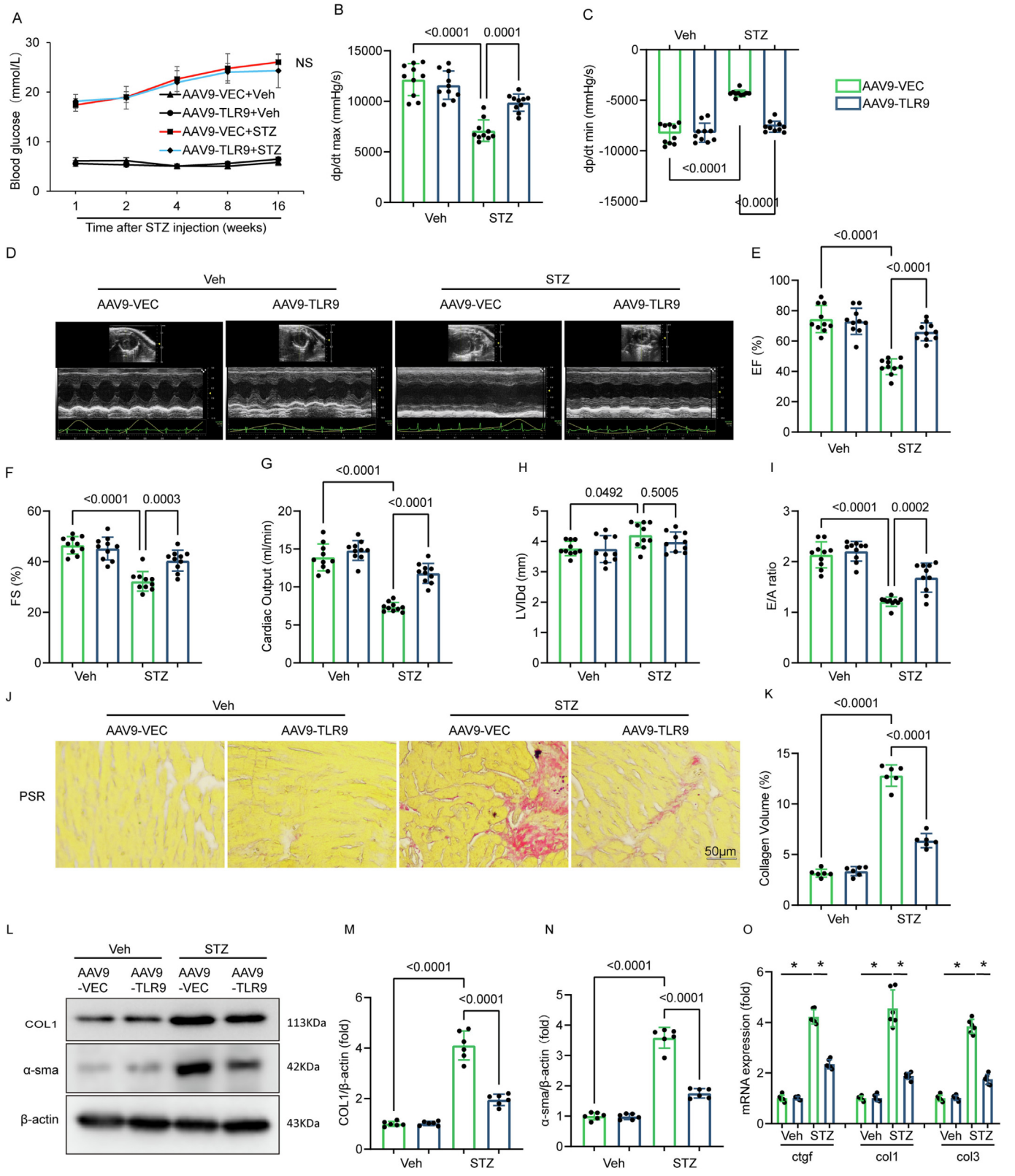

Fig. 2. TLR9 overexpression attenuates cardiac dysfunction and fibrosis in diabetic mice. A. Blood glucose of mice at duration of diabetes (n = 10); B-C. hemodynamic measurements. Peak derivative of pressure overtime (+dP/dt) is the maximal value of the instantaneous first derivative of left ventricular pressure; minimum peak derivative of pressure over time (-dP/dt) is the minimum value of the instantaneous first derivative of left ventricular pressure (n = 10); D-I. Representative B-model and M−model echocardiography in mice and cardiac function presented as ejection fraction (EF), fractional shortening (FS), cardiac output, left ventricular diastolic diameter (LVIDd) and E/A ratio (n = 10); J-K. Representative images of Sirius red staining and quantification of fibrotic area in cardiac tissues (n = 6); L-N. Immunoblotting blot analysis of Col-Ⅰand α-sma protein levels in cardiac tissues; O. The mRNA levels of *ctgf, col 1,col 3* in the cardiac tissues (n = 6). Significance was assessed by one-way ANOVA and Tukey's post hoc test. Data are shown as the mean ± SEM. (For interpretation of the references to colour in this figure legend, the reader is referred to the web version of this article.)

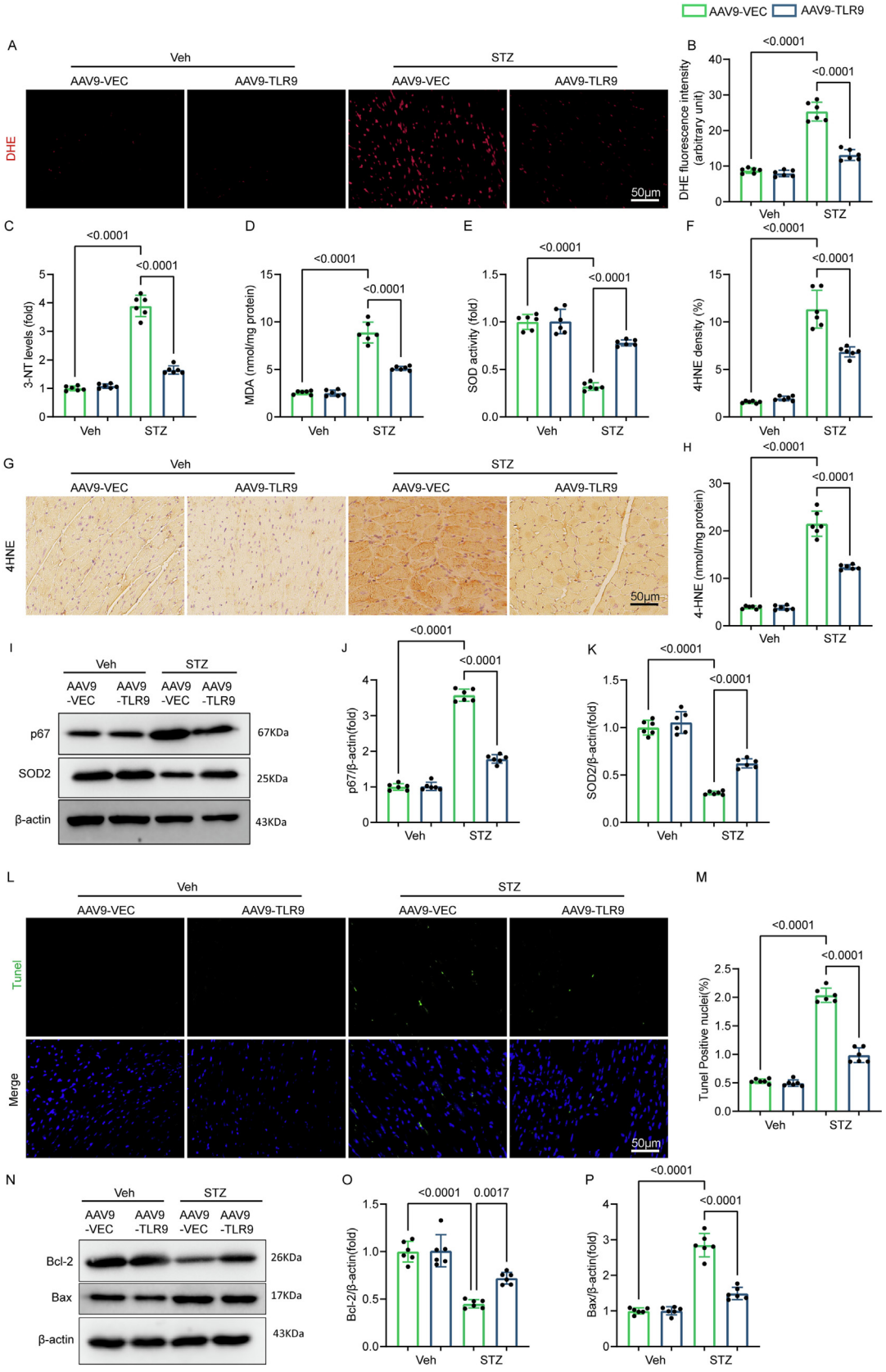

Fig. 3. TLR9 overexpression alleviates diabetes-induced oxidative injury and apoptosis. A-B. Representative images of DHE staining in the cardiac tissues and quantification of the corresponding fluorescence intensity (n = 6); C. 3-NT levels in cardiac tissues (n = 6); D. MDA levels in cardiac tissues (n = 6); E. 4-HNE levels in cardiac tissues (n = 6); F. SOD activity in cardiac tissues (n = 6); G-H. Representative images and quantification (n = 6, 10 + fields per heart) of 4-HNE Immunohistochemistry staining in diabetic hearts; I-K. Western blot analysis of p67phox and SOD2 in diabetic mice hearts (n = 6); L-M. TUNEL assay by double staining with DAPI (blue) and TUNEL (green) detected apoptotic cells in mouse hearts. The quantification of TUNEL positive nuclei is shown (n = 6); N-P. Representative western blot and analysis of Bcl-2, Bax in diabetic hearts (n = 6). Significance was assessed by one-way ANOVA and Tukey's post hoc test. Data are shown as the mean ± SEM. (For interpretation of the references to colour in this figure legend, the reader is referred to the web version of this article.)

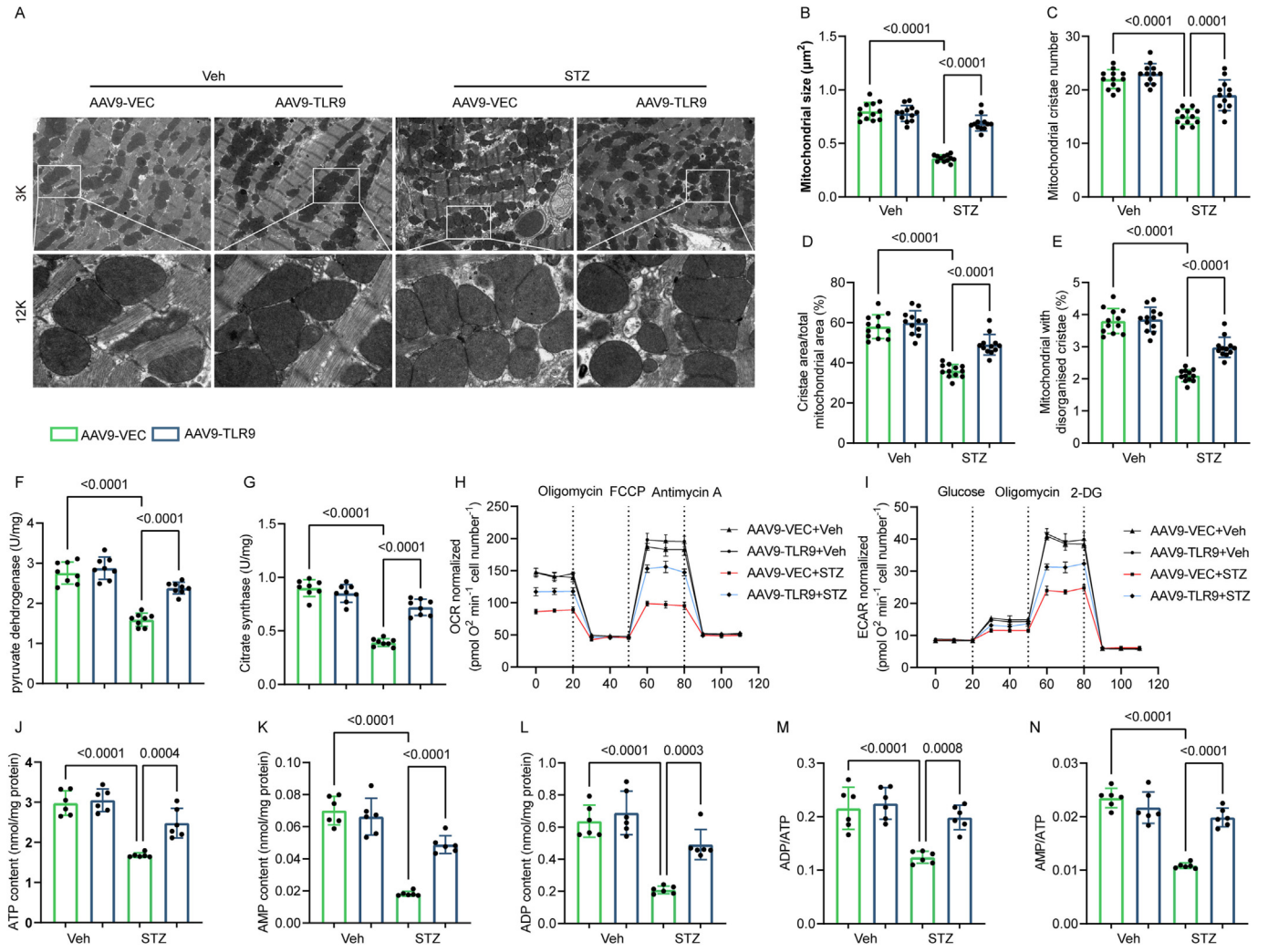

Fig. 4. TLR9 reinstates mitochondrial function and reduces energy substrates in the Mouse Model of Diabetes. A. Representative transmission electron microscopic images of mitochondria in mice treated with vehicle or STZ (magnification × 3000 [3 K], scale bar 5 μm; ×12,000 [12 K], scale bar 1 μm); B-E. Quantitative analysis of mitochondrial size, mitochondrial cristae number, cristae area and the proportion of mitochondria with disorganised cristae. (n = 12); F-G. Activity of pyruvate dehydrogenase (PDH) and citrate synthase (CS) were analyzed in heart tissues from indicated mice (n = 8); H, Oxygen consumption rate (OCR) in AMCMs isolated from indicated mice (n = 6); I, Extracellular flux analyzer traces of a glycolysis stress measured as the extracellular acidification rate (ECAR) in AMCMs isolated from indicated mice (n = 6); J-N. Measurements of ATP, ADP, AMP, ADP/ATP ratio and AMP/ATP ratio in cardiac tissues (n = 6). Significance was assessed by one-way ANOVA and Tukey's post hoc test. Data are shown as the mean ± SEM.

immunofluorescence of Nrf2 (Fig. 5**A, 5D–5F, 5K**). However, despite the significant role of NOX2/4 in the control of oxidative stress, overexpression of TLR9 had little effect on their expression in response to DCM [38] (Fig. 5**A, 5G–5H**).

We also conducted cell experiments to validate the in vivo findings. NRCMs were overexpressed TLR9 using adenovirus transfection technology, and the transfection results were verified by WB (**Fig. S4A**). Consistent with the in vivo results, AMPKα2 phosphorylation and PGC-1α expression were significantly reduced in high glucose-stimulated cardiomyocytes, but were significantly enhanced after TLR9 overexpression (**Fig. S4B–S4D**). Moreover, the levels of Nrf2 and HO-1 protein expression in cardiomyocytes were significantly higher in the HG + AdTLR9 group than in the HG group, although they were significantly lower in the HG group compared to the control group (**Fig. S4B, S4E–S4G**). Similar to the in vivo experiments, TLR9 overexpression did not reduce the HG-induced elevation of Nox2/4 expression (**Fig. S4B, S4H-S4I**). Overall, these data indicate that TLR9 participates in nuclear translocation, Nrf2 activation, and PGC-1α activation both in vivo and in vitro.

TLR9-Mediated protective role on HG-Stimulated primary cardiomyocytes via AMPK- PGC-1α pathway

In NRCMs, we assessed ROS levels and cell viability in the presence or absence of AMPK inhibitors or PGC-1α inhibitors to elucidate the role of AMPK and PGC-1α in TLR9-mediated preservation of energy metabolism and cell injury. Our data revealed a significant increase in intracellular ROS levels in NRCMs exposed to HG compared to control groups. TLR9 overexpression nearly abolished HG-induced ROS production, and this protective effect of TLR9 was attenuated by either the AMPK inhibitor (Dors) or the PGC-1α antagonist (SR-18292) (**Fig. S5A-S5B**). Similarly, the beneficial effects of TLR9 on increasing cell viability in HG-stimulated cardiomyocytes were diminished by the presence of inhibitors for either AMPK or PGC-1α (**Fig. S5C**).

Furthermore, HG led to decreased AMPK phosphorylation and expression of PGC-1α, Nrf2, HO-1, BCL-2, and SOD2, but increased the expression of BAX and P67phox, which were substantially restored with TLR9 overexpression (**Fig. S5D–S5L**). Notably, the effect of TLR9 on restoring PGC-1α expression was abolished by

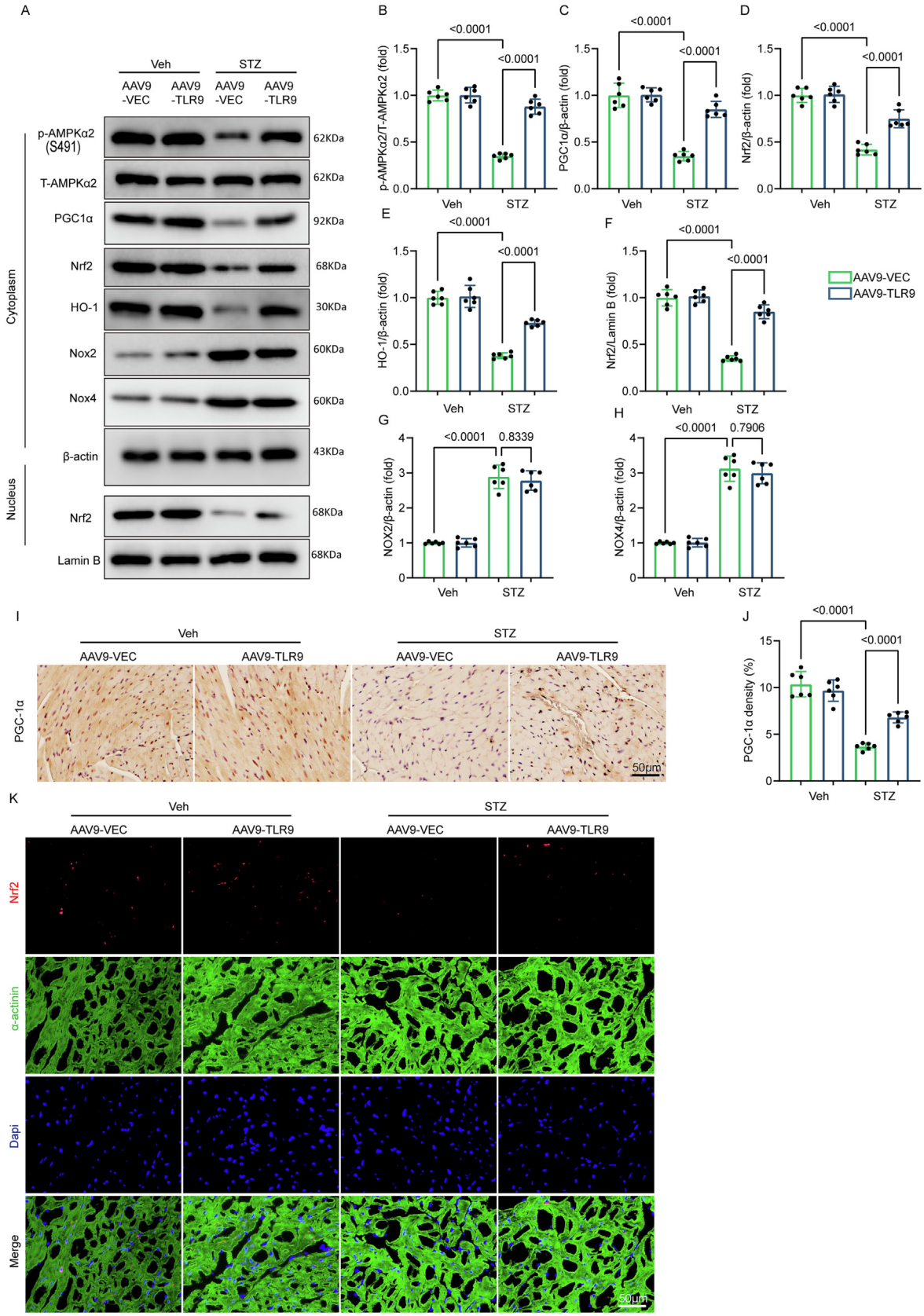

Fig. 5. TLR9 promotes PGC-1α activation and Nrf2 activation and nuclear translocation in vivo A-H. Western blot analysis (left panel) and densitometric quantification (right panel) of phosphorylated AMPKα2, total AMPKα2, PGC-1α, Nrf2, HO1, Nox2, Nox4 in cardiac tissues of each group (n = 6); I-J. Representative images and quantification (n = 6, 10 + fields per heart) of PGC-1α in mice hearts (n = 6); K. Representative images of immunofluorescence of Nrf2 (red) and α-actinin (green) in cardiac tissues. Significance was assessed by one-way ANOVA and Tukey's post hoc test. Data are shown as the mean ± SEM. (For interpretation of the references to colour in this figure legend, the reader is referred to the web version of this article.)

the AMPK antagonist (Fig. S5**D, S5F**). Additionally, the PGC-1α inhibitor significantly reduced the positive effects of TLR9 on Nrf2, HO-1, BCL-2, SOD2, BAX, and P67phox expression in NRCMs, but did not affect AMPK phosphorylation (Fig. S5**D–S5E, S5G–S5L**). Taken together, these findings suggest that TLR9 exerts its positive impact on HG-stimulated NRCMs through the activation of PGC-1α via the AMPK pathway.

AMPKA or PGC-1α deficiency abolish the protective effect of TLR9 against DCM

Wild-type (WT) and AMPKα2 knockout mice (AMPKα2$^{-/-}$) were used to further demonstrate whether AMPK activation mediated the protective effects of TLR9 against DCM (Fig. S6**A**). To create the DCM model, AAV9-TLR9 was overexpressed in the myocardium and was injected in situ before being injected with STZ (Fig. S6**B**). Mice in the AMPKα2$^{-/-}$+AAV9-VEC + STZ and AMPKα2$^{-/-}$+AAV9-TLR9 + STZ group demonstrated a worsened systolic and diastolic dysfunction, as shown by decreased EF and FS, restricted LVIDd, lower E/A ratio, and TLR9 overexpression did not enhance cardiac function in AMPKα2$^{-/-}$ mice (Fig. S6**D–S6G**). As expected, PSR staining demonstrated that AMPKα2 deficiency balances the impact of TLR9 on reducing STZ-induced cardiac collagen deposition (Fig. S6**H–6I**). DHE staining of heart demonstrated that TLR9 lowered myocardial ROS levels in the WT-STZ mice but not in AMPKα2$^{-/-}$- STZ mice (Fig. S6**H, 6J**). Additionally, AMPKα2 deficiency eliminated TLR9′s effect on reducing cardiomyocyte apoptosis (Fig. S6**H, S6K**).

Correspondingly, we subsequently employed PGC-1α-cKO mice to explore the impact of PGC-1α on TLR9-mediated cardioprotection. We crossbred αMHC-Cre and PGC-1α(flox/flox) mice to obtain the αMHC-Cre; PGC-1α((fl/fl) mice (Fig. S7**A–S7D**). As expected, systolic and diastolic dysfunctions and collagen deposition were comparably found in WT- and PGC-1α-cKO animals. TLR9 overexpression corrected these cardiac structural changes, fibrosis, and cardiac dysfunction in the WT-STZ mice but not in PGC-1α-cKO – STZ mice (Fig. S8**A-S8G**). Similarly, DHE labeling showed that TLR9 reduced cardiac ROS levels in WT-STZ mice but not in PGC-1α-cKO-STZ animals (Fig. S8**F, S8H**). TUNEL staining results demonstrated that PGC-1α depletion in heart reversed the protective role against myocardial apoptosis (Fig. S8**F, S8I**). Collectively, our findings demonstrated that PGC-1α and AMPK were responsible for mediating TLR9′s protective effects against cardiac dysfunction and injury brought on by diabetes.

Triad3A interacts with TLR9 and promotes K48-Linked ubiquitination

The regulation mechanism of TLRs signal transduction includes positive regulation and nuclear negative regulation. Currently, negative regulation (i.e., the reduction of TLRs signal transduction) is mainly found to interfere with the formation of the junction complex to block the signal transduction pathway and the regulation of the transcription level [50]. In response to the decreased expression of TLR9 in the DCM state, we speculate that it changes at two levels, mRNA and protein levels. After detecting its mRNA expression at the transcriptional level, it was found that the mRNA level of TLR9 did not change significantly (Fig. 6**A**). Therefore, we focused our research on the ubiquitination and degradation of TLRs. A previous study found that Triad3A negatively regulates TLR4 and TLR9-mediated MyD88-dependent NF-κB activation and AKT phosphorylation in pressure overload-induced cardiac hypertrophy [16]. Subsequently, we evaluated the protein expression of Triad3A. Interestingly, DCM led to a substantial increase in Triad3A protein expression (Fig. 6**B**).

To determine if TLR9 is a substrate of the E3 ligase Triad3A, we conducted immunoblotting experiments and confirmed that the ubiquitination of TLR9 was elevated in NRCMs with Triad3A overexpression and following HG administration. Moreover, in myocardial cells from mice treated with STZ, the levels of ubiquitinated TLR9 were higher compared to those from control mice (Fig. 6**C–6E**). These results suggest that Triad3A plays a role in the ubiquitination of TLR9, which may contribute to the observed decrease in TLR9 expression in the context of diabetic cardiomyopathy.

The function of Triad3A in regulating TLR9 protein stability was further assessed in 293 T cells. A reciprocal coimmunoprecipitation (co-IP) study demonstrated a specific interaction between TLR9 and Triad3A (Fig. 6**F**). Additionally, the GST precipitation assay confirmed the physical interaction between TLR9 and Triad3A (Fig. 6**G**). Gradual overexpression of Triad3A led to a progressive decrease in TLR9 expression (Fig. S9**A**). Conversely, Triad3A silencing significantly increased the expression of TLR9 (Fig. S9**B**).

To investigate whether Triad3A reduces TLR9 expression by inhibiting TLR9 transcription or promoting TLR9 proteasomal degradation, we used the protein synthesis inhibitor CHX and the proteasome inhibitor MG132 in 293 T cells. The results showed that TLR9 expression decreased over time in a CHX-dependent manner in both the control siRNA group and the Triad3A siRNA group **(**Fig. S9**C**), indicating that Triad3A did not affect the synthesis of TLR9 protein. Furthermore, in both groups, TLR9 expression increased over time in response to MG132 treatment. However, the rate and extent of TLR9 expression increase were higher in the control siRNA group compared to the Triad3A siRNA group (Fig. S9**D**), suggesting that Triad3A inhibits TLR9 expression by promoting proteasome-mediated degradation of TLR9.

Next, to evaluate if Triad3A causes TLR9 degradation via TLR9 polyubiquitination, coimmunoprecipitation was done to determine the ubiquitination impact of Triad3A on TLR9 in 293 T cells. The results demonstrated that in the presence of MG132, the interaction between exogenous Triad3A and TLR9, as well as the interaction between endogenous Triad3A and TLR9, was greatly strengthened (Fig. S9**E-S9F**) Consistent with these observations, overexpression of Triad3A dramatically raised the amount of TLR9 polyubiquitination in the presence of MG132 **(**Fig. S9**G).** Conversely, knocking down Triad3A in the presence of MG132 led to a reduction in TLR9 polyubiquitination (Fig. S9**H**). These results collectively indicate that Triad3A promotes the polyubiquitination of TLR9, thereby facilitating TLR9 degradation through the ubiquitin–proteasome pathway.

The screening of mutant variants of ubiquitin for potential lysine ubiquitination types revealed that under HG treatment, both wild-type (WT) Ub and K48O (Ub with intact Lys48 residue alone) could be conjugated to TLR9 by Triad3A, whereas K6O, K11O, K27O, or K63O showed no such connection **(**Fig. 6**H**). Triad3A additionally failed to bind K48R (Ub just Lys48 residue was altered) to TLR9 (Fig. 6**I**), demonstrating that Triad3A primarily promoted K48-linked ubiquitination on TLR9.

Furthermore, overexpression of Triad3A exacerbated cycloheximide-induced TLR9 degradation (Fig. 6**J**), which was prevented by MG132 (Fig. 6**K**). Overall, Triad3A binds with TLR9 preferentially and facilitates its proteasomal degradation by catalyzing K48-linked ubiquitination in the presence of HG.

Inhibition of Triad3A attenuates diabetic cardiac injury

Our results showed that Triad3A inhibition and its signal transduction pathway suppression would be a useful treatment strategy for DCM. We investigated siTriad3A's possible impact on experimental DCM (Fig. S10**A**). We measured intracellular ROS levels and discovered that siTriad3A could suppress HG-stimulated ROS generation but not in TLR9-KO myocytes (Fig. S10**B-S10C**). Additionally, siTriad3A's effects on improving cell survival in HG-treated cardiomyocytes were reversed by TLR9 deficiency

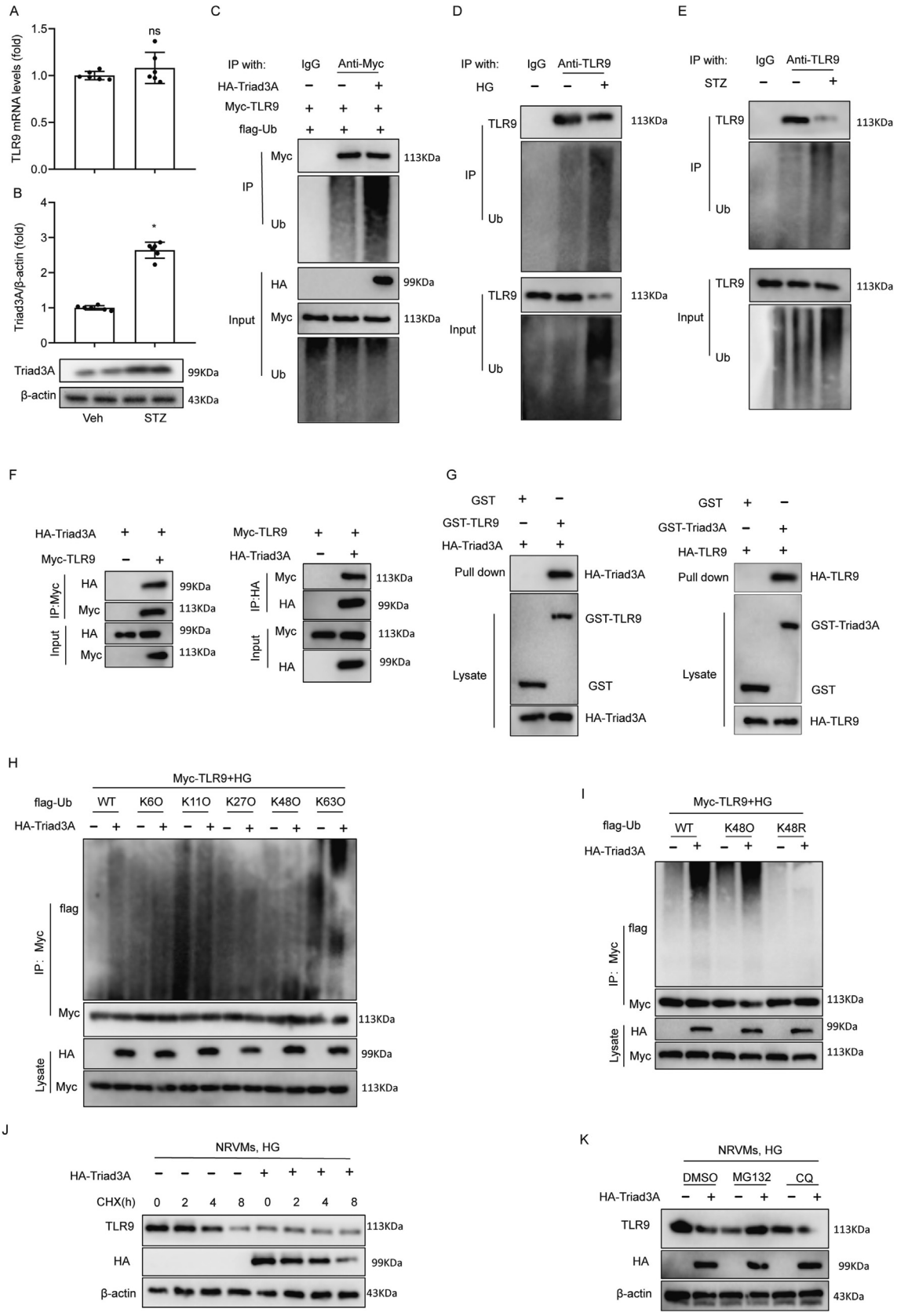
A
TLR9 mRNA levels (fold)
ns
B
Triad3A/β-actin (fold)
*
Triad3A
β-actin
99KDa
43KDa
Veh
STZ
C
IP with: IgG Anti-Myc
HA-Triad3A
Myc-TLR9
flag-Ub
IP
Myc
Ub
Input
HA
113KDa
99KDa
D
IP with: IgG Anti-TLR9
HG
TLR9
E
STZ
F
HA-Triad3A
Myc-TLR9
IP:Myc
IP:HA
G
GST
GST-TLR9
HA-Triad3A
Pull down
Lysate
GST-Triad3A
HA-TLR9
H
Myc-TLR9+HG
flag-Ub
WT
K6O
K11O
K27O
K48O
K63O
flag
I
K48R
J
NRVMs, HG
CHX(h)
0 2 4 8 0 2 4 8
K
DMSO
MG132
CQ

(**Fig. S10D**). Following HG administration, ATP, AMP, ADP content, and the AMP/ATP, ADP/ATP ratio were decreased. TLR9 KO prevented siTriad3A's positive effects on these parameters (**Fig. S10-E-S10I**). Additionally, HG caused other abnormalities such as decreased P-AMPK and PGC-1α expression, while TLR9 KO eliminated the protective effects of Triad3A silence (**Fig. S10J–S10L**).

We used shRNA for loss-of-function studies to investigate Triad3A's involvement in controlling diabetic heart damage. In line with predictions, Triad3A silencing in cardiomyocytes reduced cardiac fibrosis, oxidative stress, apoptosis, and dysfunction in WT-STZ animals but not in TLR9-KO mice (Fig. 7**A-10I**). In WT-STZ mice but not in TLR9-KO mice, silencing Triad3A dramatically raised ATP, AMP, and ADP levels as well as the ratios of AMP/ATP and ADP/ATP (Fig. 7**J-7 N**). Finally, it was found that lower levels of P-AMPK and PGC-1α were present in the hearts of STZ mice. These changes were restored by Triad3A inhibition in WT-STZ mice, but were abolished in TLR9-KO-STZ animals (Fig. 7**O-7Q**). These data indicated that Triad3A is essential for TLR9 function and diabetic cardiac injury.

These findings, when considered collectively, imply that TLR9 is an important target of Triad3A, and addressing the Triad3A-TLR9 axis might give therapeutic methods for diabetic heart damage.

Discussion

TLR9 has been implicated not only in the etiology of autoimmune diseases [39] but also in the pathophysiology of cardiometabolic disorders such as obesity and atherosclerosis [40,41]. To recreate the pathophysiology of DCM, myocardial cells activated by high glucose were used to establish an in vitro diabetes model, while an in vivo type 1 DCM model was generated through intraperitoneal injection of STZ. In both high-glucose-stimulated cardiomyocytes and STZ-induced mouse cardiomyocytes, TLR9 expression was significantly decreased. Under the stimulation of STZ or HG, elevated Triad3A leads to the K48-linked ubiquitination and degradation of TLR9. Decreased expression of TLR9 results in alterations in mitochondrial structure and function, accompanied by a reduction in the AMP/ATP ratio, subsequently inhibiting the AMPK/PGC-1α signaling pathway, and exacerbating the pathological conditions in mice, such as oxidative stress and cell apoptosis. However, it does not have an effect on the inflammatory response and signaling pathways. As a consequence, diabetic mice experience cardiac remodeling and cardiac dysfunction. Conversely, cardiac-specific overexpression of TLR9 can counteract the aforementioned pathological changes by maintaining mitochondrial structure and function, thereby ameliorating cardiac remodeling and improving heart function. (Fig. 7**R**).

TLR9 plays a well-established role in cardiovascular disease. Studies on TLR9-deficient (TLR9-KO) mice have shown that pressure overload-induced cardiac dysfunction and inflammation are improved in these mice [42]. Inhibition of sterile inflammation mediated by TLR9-NF-κB signaling has also been reported to improve right heart dysfunction induced by pulmonary artery ligation in rats [43]. Conversely, injection of CpG-ODN (a TLR9 agonist) has been found to exacerbate myocardial infarction and impair cardiac function and survival following ischemia–reperfusion injury [44]. TLR9 deficiency, however, was shown to increase mortality in a model of heart failure in SERCA2aKO mice, while having no effect on cardiac function, structure, or biochemical parameters [45]. Our previous work demonstrated that TLR9-KO dramatically reversed the decline in cardiac function induced by doxorubicin [46]. On the other hand, TLR9 overexpression has been associated with positive outcomes in certain contexts. For instance, B cell-specific TLR9 overexpression significantly improved nephritis, contrasting the effect of TLR9 knockdown [47]. Interestingly, TLR9 activation has been found to protect cardiomyocytes from ischemia-induced damage by regulating energy metabolism. Pretreatment with CpG-ODN was shown to boost TLR9 expression in cardiomyocytes and regulate metabolism [8,9,28]. Our findings add to the existing knowledge on the complex role of TLR9 in cardiovascular disease. While TLR9 deficiency can improve certain aspects of cardiac dysfunction and inflammation, TLR9 activation, especially in a cardiac-specific context, appears to be protective against deterioration in cardiac function, particularly in the context of DCM. However, further research is needed to fully elucidate the mechanisms and potential interplay between TLR9, energy metabolism, and islet function in the context of cardiovascular disease. Studies on TLR9 and islet function have revealed that TLR9-deficient mice have more islets, more islet beta cells, increased glucose-stimulated insulin secretion in vitro, and improved glucose tolerance in vivo [6]. The specific targeting of insulin-producing islet cells by STZ, used to induce diabetes in our study, might explain this phenomenon.

TLR9 plays a role in modulating the inflammatory response, thereby reducing stress-induced cardiac hypertrophy [48]. Activation of TLR9 in hematopoietic cells has been associated with increased adipose tissue inflammation and insulin resistance, as shown in in vitro studies [49]. Interestingly, our research revealed that overexpression of TLR9 did not augment STZ-induced inflammation levels and pathways, contrary to its canonical role in inflammation regulation. This suggests that TLR9 may have distinct inflammatory functions in immune cells, which could explain its limited impact on inflammation in this context [28].

Instead, TLR9 appears to primarily regulate cardiac energy metabolism to enhance heart function and mitigate pathological changes in diabetic conditions. In both diabetic patients and diabetic animal models, cardiac mitochondrial dysfunction, oxidative stress, and abnormal mitochondrial ultrastructure have been observed, leading to disease progression [50]. Physiologically, the integrity of mitochondrial structure is crucial for mitochondrial energy generation. However, defective mitochondrial structure can exacerbate the decline of $\Delta\Psi m$, leading to cytochrome *c* leakage and mitochondrial dysfunction [51], which is considered a primary source of ROS production and a key contributor to DCM [52,53]. Our data confirm that TLR9 overexpression significantly reduces abnormal cardiac mitochondrial morphology in the context of diabetes and maintains the AMP/ATP ratio. The disruption of cardiac energy metabolism is considered a crucial factor in the cardiac complications of diabetes [54], as alterations in ATP production adversely affect cardiac function in DCM. TLR9 activation

Fig. 6. Triad3A interacts with TLR9 and promotes K48-linked ubiquitination A. The mRNA of TLR9 in cardiac tissues from healthy and diabetic mice (n = 6); B. Representative western blot analysis of Triad3A in cardiac tissues from healthy and diabetic mice (n = 6); C. Immunoblots of the ubiquitinated tlr9 after Triad3A overexpression; D. Immunoblots of the ubiquitinated TLR9 in NRCMs treated with or without HG; E. Immunoblots of the ubiquitinated TLR9 in myocardial cells treated with or without STZ; F. Coimmunoprecipitation (coIP) assays were performed to examine the interaction of Triad3A and TLR9 in 293 T cells transfected with the indicated plasmids; G. GST pull-down assays showing the interaction Triad3A and TLR9 in 293 T cells transfected with the indicated plasmids. H-I. In screening for potential lysine ubiquitination types, the ubiquitination of Myc-TLR9 in response to Triad3A overexpression was examined in NRCMs transfected with the wild-type (WT) and mutated Myc-Ub plasmids and treated with HG. J. Immunoblotting analysis of TLR9 in NRCMs infected with HA-Triad3A and treated with HG (20 μM) for 24 h and cycloheximide (CHX, 50 μM) for the indicated time points. K, Immunoblotting analysis of TLR9 in NRCMs after Triad3A overexpression for 24 h and treatment with HG for 24 h, dimethyl sulfoxide (DMSO), MG132 (50 μM) or chloroquine (CQ, 50 μM) for 6 h.

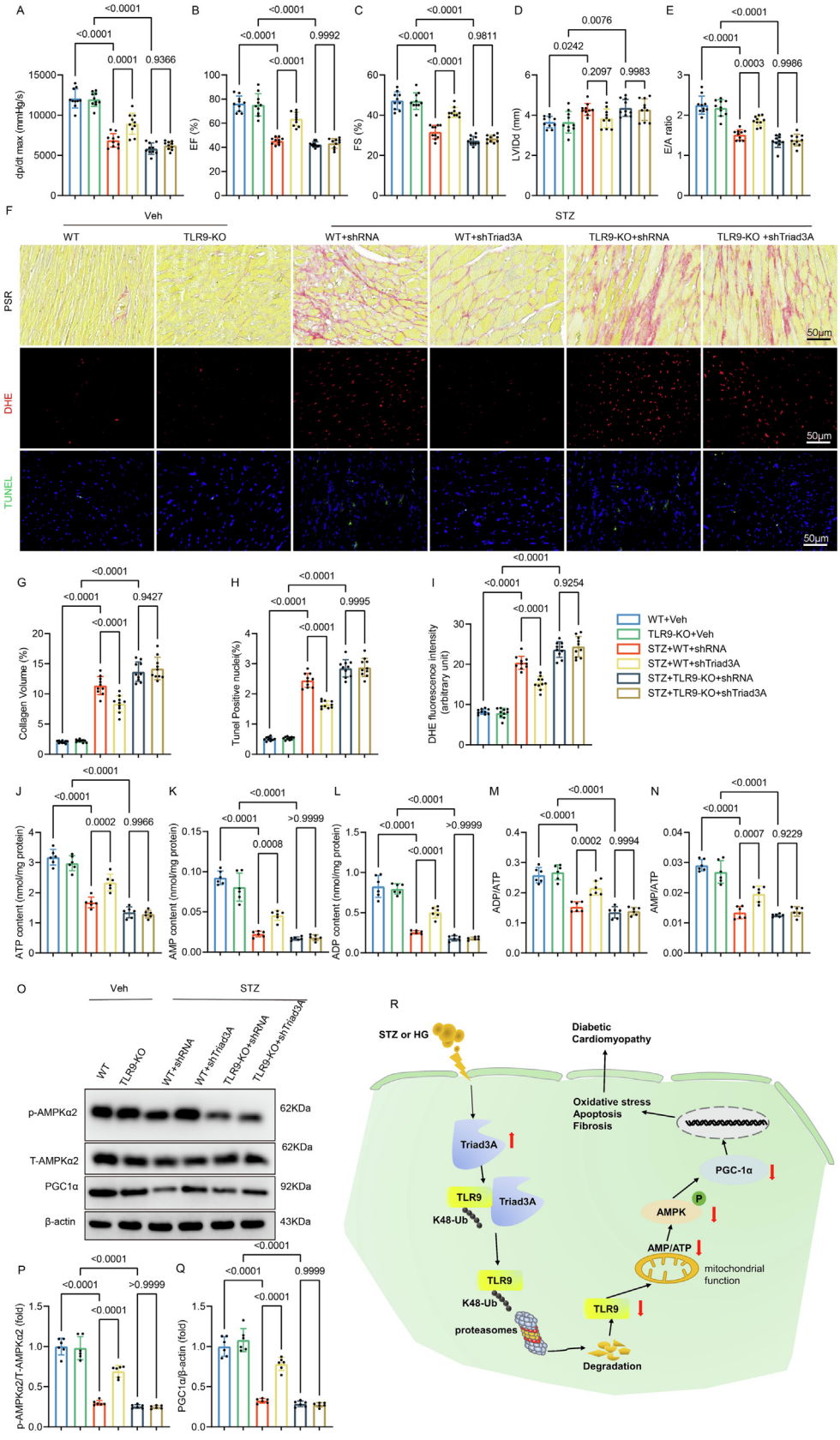
A
B
C
D
E
dp/dt max (mmHg/s)
EF (%)
FS (%)
LVIDd (mm)
E/A ratio
F
Veh
STZ
WT
TLR9-KO
WT+shRNA
WT+shTriad3A
TLR9-KO+shRNA
TLR9-KO +shTriad3A
PSR
DHE
TUNEL
50μm
G
H
I
Collagen Volume (%)
Tunel Positive nuclei(%)
DHE fluorescence intensity (arbitrary unit)
WT+Veh
TLR9-KO+Veh
STZ+WT+shRNA
STZ+WT+shTriad3A
STZ+TLR9-KO+shRNA
STZ+TLR9-KO+shTriad3A
J
K
L
M
N
ATP content (nmol/mg protein)
AMP content (nmol/mg protein)
ADP content (nmol/mg protein)
ADP/ATP
AMP/ATP
O
p-AMPKα2
T-AMPKα2
PGC1α
β-actin
62KDa
62KDa
92KDa
43KDa
P
Q
p-AMPKα2/T-AMPKα2 (fold)
PGC1α/β-actin (fold)
R
STZ or HG
Diabetic Cardiomyopathy
Oxidative stress
Apoptosis
Fibrosis
Triad3A
TLR9
K48-Ub
proteasomes
Degradation
PGC-1α
AMPK
P
AMP/ATP
mitochondrial function

seems to confer increased cardiomyocyte tolerance to hypoxic stress by modulating energy substrates, resulting in elevated AMP/ATP ratio and subsequent activation of AMPK, without triggering typical inflammatory responses [28]. Preconditioning with CpG-ODN, a TLR9 agonist, has been shown to protect cardiac function by modulating cardiomyocyte energy metabolism [8]. In line with these findings, our study demonstrated that TLR9 overexpression significantly increased the AMP/ATP ratio in myocardial tissue.

In the context of diabetes, the upregulation of Triad3A leads to an increase in TLR9 ubiquitination and subsequent degradation, resulting in decreased TLR9 expression and attenuated signal transduction. Conversely, when Triad3A is silenced using small interfering RNA, the ubiquitination of TLR9 is reduced, leading to enhanced signal transduction mediated by TLR9. Additionally, Triad3A targets the adapter protein TRAF3 for proteasomal degradation through K48-linked ubiquitin-mediated degradation, negatively regulating the RIG-I-like receptor pathway [55]. The present study further demonstrates the interaction between Triad3A and TLR9, which facilitates the proteasomal degradation of TLR9 via K48-linked ubiquitination. In our investigation, the downregulation of Triad3A expression effectively improved cardiac function and mitigated pathological changes associated with DCM, primarily mediated through the TLR9 pathway.

Our study reveals the interaction between TLR9 and Triad3A, which plays a critical role in the pathogenesis of diabetic cardiomyopathy. These findings offer potential new therapeutic targets for clinical intervention. By modulating the interaction between TLR9 and Triad3A, we may be able to regulate the AMPK/PGC-1α signaling pathway, thus mitigating myocardial damage and improving cardiac function in diabetic cardiomyopathy. These research outcomes provide promising new strategies for the treatment of diabetic cardiomyopathy. Given the complexity and individual variability of diabetic cardiomyopathy, personalized treatment strategies are of utmost importance. In our study, we observed variations in TLR9 expression levels among different individuals, suggesting the possibility of personalized treatment opportunities. By integrating patients' genomic information and physiological characteristics, we may identify those who are suitable candidates for TLR9-targeted therapies, leading to more precise and effective treatment approaches. And there have been clinical studies on TLR9 targets. Activation of TLR9 inhibits Th17 cells and induces anti-inflammatory IL10 + macrophages and regulatory T cells, thereby improving the dysregulated intestinal cytokine balance [56]. TLR9 agonist MGN1703 regulates human lymph node B cells in vivo. These findings provide further considerations for the development of TLR9 agonists as immunotherapies against cancer and infectious diseases [57]. In a phase Ib study involving patients with advanced melanoma, the intratumoral TLR9 agonist vidutolimod plus pembrolizumab had a manageable safety profile and showed promising clinical activity [58]. Although our study is still in its early stages and requires further clinical validation, we hold an optimistic view of the potential of TLR9-Triad3A interaction as a therapeutic approach for diabetic cardiomyopathy. As research advances and clinical trials progress, we anticipate translating these research findings into more specific and effective treatment modalities, ultimately improving the quality of life and prognosis for patients.

Conclusion

In conclusion, our study provides valuable insights into the regulatory mechanism of TLR9 in DCM. TLR9 plays a crucial role in maintaining cardiac function and mitigating pathological alterations in the diabetic heart through its impact on mitochondrial structure and function, energy metabolism, oxidative stress, and apoptosis. The upregulation of Triad3A in the diabetic state leads to increased ubiquitination and degradation of TLR9, resulting in reduced TLR9 expression and impaired signal transduction. By investigating the interplay between TLR9 and Triad3A, we have uncovered a novel mechanism underlying TLR9 regulation and its impact on cardiac function. The downregulation of Triad3A expression represents a promising therapeutic approach for ameliorating cardiomyocyte energy metabolism, alleviating oxidative stress, and improving cardiac function in DCM.

Our findings highlight the importance of TLR9 as a potential therapeutic target for the treatment of diabetic cardiomyopathy. By understanding the intricate signaling pathways involved in TLR9 regulation, future research may lead to the development of targeted therapies to enhance TLR9 function and improve cardiac outcomes in diabetic patients. Further investigations are warranted to explore the full therapeutic potential of TLR9 modulation in the context of diabetic cardiomyopathy and other cardiovascular diseases.

Funding Sources

This work was supported by grants from the National Natural Science Foundation of China (81530012).

Compliance with Ethics Requirements

All animal experiments were performed in accordance with the Guidelines for the Care and Use of Laboratory Animals (NIH publication, revised 2011) and approved by the Animal Care and Use Committee of Renmin Hospital of Wuhan University (IACUC Issue No. WDRM20171201).

Declaration of Competing Interest

The authors declare that they have no known competing financial interests or personal relationships that could have appeared to influence the work reported in this paper.

Fig. 7. Triad3A silence inhibits STZ-induced diabetic heart injury and energy metabolism disorders through TLR9. A. hemodynamic measurements. Peak derivative of pressure overtime (+dP/dt) is the maximal value of the instantaneous first derivative of left ventricular pressure (n = 10); B-C. Echocardiographic assessment for each group (n = 10); D. left ventricular diastolic diameter (n = 10); E. E/A ratio(n = 10); F. Representative images of Sirius red staining, DHE staining, and TUNEL staining in cardiac tissues. G. Quantification of fibrotic area (n = 10); H. Quantification of the DHE fluorescence intensity (n = 10); I. Quantification of the TUNEL positive nuclei (n = 10); J-N. Measurements of ATP, ADP, AMP, ADP/ATP ratio, and AMP/ATP ratio in cardiac tissues. O-Q. Western blot analysis (left panel) and densitometric quantification (right panel) of phosphorylated AMPKα2, total AMPKα2, PGC-1α in cardiac tissues (n = 6). Significance was assessed by one-way ANOVA and Tukey's post hoc test. Data are shown as the mean ± SEM. R. Graphical Abstract: Triad3A elevation induced by STZ or HG stimulation leads to degradation of TLR9 K48-linked proteasomal ubiquitination, which impairs mitochondrial function and reduces the AMP/ATP ratio and inhibits the activation of AMPK and PGC-1, which in turn leads to oxidative stress, apoptosis and fibrosis and other pathological changes. STZ: Streptozotocin; HG: High glucose; TLR9: Toll-like receptor 9; AMP: Adenosine monophosphate; ATP: Adenosine triphosphate; AMPK: Adenosine 5'-monophosphate (AMP)-activated protein kinase; PGC-1α: Peroxisome-proliferator-activated receptorγcoactivator-1α. (For interpretation of the references to colour in this figure legend, the reader is referred to the web version of this article.)

Appendix A. Supplementary data

Supplementary data to this article can be found online at https://doi.org/10.1016/j.jare.2023.08.015.

References

[1] Nirengi S, Peres Valgas da Silva C, Stanford KI. Disruption of energy utilization in diabetic cardiomyopathy; a mini review. Curr Opin Pharmacol 2020;54:82–90.
[2] Dillmann WH. Diabetic Cardiomyopathy. Circ Res 2019;124(8):1160–2.
[3] Wang ZV, Hill JA, Hill JA. Diabetic cardiomyopathy: catabolism driving metabolism. *Circulation* 2015;131(9):771–3.
[4] Karulin AY, Hesse MD, Yip HC, Lehmann PV. Indirect IL-4 pathway in type 1 immunity. J Immunol 2002;168(2):545–53.
[5] Boyd JH, Mathur S, Wang Y, Bateman RM, Walley KR. Toll-like receptor stimulation in cardiomyoctes decreases contractility and initiates an NF-kappaB dependent inflammatory response. Cardiovasc Res 2006;72 (3):384–93.
[6] Liu M, Peng J, Tai N, Pearson JA, Hu C, Guo J, et al. Toll-like receptor 9 negatively regulates pancreatic islet beta cell growth and function in a mouse model of type 1 diabetes. Diabetologia 2018;61(11):2333–43.
[7] Sha S, Pearson JA, Peng J, Hu Y, Huang J, Xing Y, et al. TLR9 Deficiency in B Cells Promotes Immune Tolerance via Interleukin-10 in a Type 1 Diabetes Mouse Model. Diabetes 2021;70(2):504–15.
[8] Zhou D-C, Su Y-H, Jiang F-Q, Xia J-B, Wu H-Y, Chang Z-S, et al. CpG oligodeoxynucleotide preconditioning improves cardiac function after myocardial infarction via modulation of energy metabolism and angiogenesis. J Cell Physiol 2018;233(5):4245–57.
[9] Shintani Y, Drexler HC, Kioka H, Terracciano CM, Coppen SR, Imamura H, et al. Toll-like receptor 9 protects non-immune cells from stress by modulating mitochondrial ATP synthesis through the inhibition of SERCA2. EMBO Rep 2014;15(4):438–45.
[10] Duerr GD, Wu S, Schneider ML, Marggraf V, Weisheit CK, Velten M, et al. CpG postconditioning after reperfused myocardial infarction is associated with modulated inflammation, less apoptosis, and better left ventricular function. Am J Phys Heart Circ Phys 2020;319(5):H995–H1007.
[11] Omiya S, Omori Y, Taneike M, Protti A, Yamaguchi O, Akira S, et al. Toll-like receptor 9 prevents cardiac rupture after myocardial infarction in mice independently of inflammation. Am J Phys Heart Circ Phys 2016;311(6): H1485–97.
[12] Krogmann AO, Lüsebrink E, Steinmetz M, Asdonk T, Lahrmann C, Lütjohann D, et al. Proinflammatory Stimulation of Toll-Like Receptor 9 with High Dose CpG ODN 1826 Impairs Endothelial Regeneration and Promotes Atherosclerosis in Mice. PLoS One 2016;11(1):e0146326.
[13] Liu Y, Nguyen PT, Wang X, Zhao Y, Meacham CE, Zou Z, et al. TLR9 and beclin 1 crosstalk regulates muscle AMPK activation in exercise. Nature 2020;578 (7796):605–9.
[14] Chuang TH, Ulevitch RJ. Triad3A, an E3 ubiquitin-protein ligase regulating Toll-like receptors. Nat Immunol 2004;5(5):495–502.
[15] Husain N, Yuan Q, Yen Y-C, Pletnikova O, Sally DQ, Worley P, et al. TRIAD3/ RNF216 mutations associated with Gordon Holmes syndrome lead to synaptic and cognitive impairments via Arc misregulation. Aging Cell 2017;16 (2):281–92.
[16] Lu X, He Y, Tang C, Wang X, Que L, Zhu G, et al. Triad3A attenuates pathological cardiac hypertrophy involving the augmentation of ubiquitination-mediated degradation of TLR4 and TLR9. Basic Res Cardiol 2020;115(2).
[17] Yuan Y-P, Ma Z-G, Zhang X, Xu S-C, Zeng X-F, Yang Z, et al. CTRP3 protected against doxorubicin-induced cardiac dysfunction, inflammation and cell death via activation of Sirt1. J Mol Cell Cardiol 2018;114:38–47.
[18] Guo Z, Fan D, Liu F-Y, Ma S-Q, An P, Yang D, et al. NEU1 Regulates Mitochondrial Energy Metabolism and Oxidative Stress Post-myocardial Infarction in Mice via the SIRT1/PGC-1 Alpha Axis. Front Cardiovasc Med 2022;9.
[19] Li Y, Feng Y-F, Liu X-T, Li Y-C, Zhu H-M, Sun M-R, et al. Songorine promotes cardiac mitochondrial biogenesis via Nrf2 induction during sepsis. Redox Biol 2021;38:101771.
[20] Low Wang CC, Hess CN, Hiatt WR, Goldfine AB. Clinical Update: Cardiovascular Disease in Diabetes Mellitus: Atherosclerotic Cardiovascular Disease and Heart Failure in Type 2 Diabetes Mellitus - Mechanisms, Management, and Clinical Considerations. Circulation 2016;133(24):2459–502.
[21] Saiyang X, Qingqing W, man X, Chen L, Min Z, Yun X, et al. Activation of Toll-like receptor 7 provides cardioprotection in septic cardiomyopathy-induced systolic dysfunction. Clin Transl Med 2021;11(1):e266.
[22] Zhang X, Hu C, Kong C-Y, Song P, Wu H-M, Xu S-C, et al. FNDC5 alleviates oxidative stress and cardiomyocyte apoptosis in doxorubicin-induced cardiotoxicity via activating AKT. Cell Death Differ 2020;27(2):540–55.
[23] Jin L, Geng L, Ying L, Shu L, Ye K, Yang R, et al. FGF21-Sirtuin 3 Axis Confers the Protective Effects of Exercise Against Diabetic Cardiomyopathy by Governing Mitochondrial Integrity. Circulation 2022;146(20):1537–57.
[24] Ma Z-G, Kong C-Y, Wu H-M, Song P, Zhang X, Yuan Y-P, et al. Toll-like receptor 5 deficiency diminishes doxorubicin-induced acute cardiotoxicity in mice. Theranostics 2020;10(24):11013–25.
[25] Ren J, Zhang N, Liao H, Chen Si, Xu L, Li J, et al. Caffeic acid phenethyl ester attenuates pathological cardiac hypertrophy by regulation of MEK/ERK signaling pathway in vivo and vitro. Life Sci 2017;181:53–61.
[26] Xie S, Chen M, Fang W, Liu S, Wu Q, Liu C, et al. Diminished arachidonate 5-lipoxygenase perturbs phase separation and transcriptional response of Runx2 to reverse pathological ventricular remodeling. EBioMedicine 2022;86:104359.
[27] Zhang Z, Yuan Y, Hu L, Tang J, Meng Z, Dai L, et al. ANGPTL8 accelerates liver fibrosis mediated by HFD-induced inflammatory activity via LILRB2/ERK signaling pathways. J Adv Res 2023;47:41–56.
[28] Shintani Y, Kapoor A, Kaneko M, Smolenski RT, D'Acquisto F, Coppen SR, et al. TLR9 mediates cellular protection by modulating energy metabolism in cardiomyocytes and neurons. PNAS 2013;110(13):5109–14.
[29] Nishimoto S, Fukuda D, Sata M. Emerging roles of Toll-like receptor 9 in cardiometabolic disorders. Inflamm Regen 2020;40(1).
[30] Drucker DJ. The Cardiovascular Biology of Glucagon-like Peptide-1. Cell Metab 2016;24(1):15–30.
[31] Carling D. The AMP-activated protein kinase cascade–a unifying system for energy control. Trends Biochem Sci 2004;29(1):18–24.
[32] Jeon SM, Chandel NS, Hay N. AMPK regulates NADPH homeostasis to promote tumour cell survival during energy stress. Nature 2012;485(7400):661–5.
[33] Puigserver P, Wu Z, Park CW, Graves R, Wright M, Spiegelman BM. A cold-inducible coactivator of nuclear receptors linked to adaptive thermogenesis. Cell 1998;92(6):829–39.
[34] Terada S, Goto M, Kato M, Kawanaka K, Shimokawa T, Tabata I. Effects of low-intensity prolonged exercise on PGC-1 mRNA expression in rat epitrochlearis muscle. Biochem Biophys Res Commun 2002;296(2):350–4.
[35] Jager S, Handschin C, St-Pierre J, Spiegelman BM. AMP-activated protein kinase (AMPK) action in skeletal muscle via direct phosphorylation of PGC-1alpha. PNAS 2007;104(29):12017–22.
[36] Nguyen T, Nioi P, Pickett CB. The Nrf2-antioxidant response element signaling pathway and its activation by oxidative stress. J Biol Chem 2009;284 (20):13291–5.
[37] Yoh K, Hirayama A, Ishizaki K, Yamada A, Takeuchi M, Yamagishi S-I, et al. Hyperglycemia induces oxidative and nitrosative stress and increases renal functional impairment in Nrf2-deficient mice. Genes Cells 2008.
[38] Chen Y-Y, Wu T-T, Ho C-Y, Yeh T-C, Sun G-C, Kung Y-H, et al. Dapagliflozin Prevents NOX- and SGLT2-Dependent Oxidative Stress in Lens Cells Exposed to Fructose-Induced Diabetes Mellitus. Int J Mol Sci 2019;20(18):4357.
[39] Honke N, Lowin T, Opgenoorth B, Shaabani N, Lautwein A, Teijaro JR, et al. Endogenously produced catecholamines improve the regulatory function of TLR9-activated B cells. PLoS Biol 2022;20(1):e3001513.
[40] Priviero F, Calmasini F, Dela Justina V, Wenceslau CF, Mccarthy CG, Webb RC. Macrophage-Specific Toll Like Receptor 9 (TLR9) Causes Corpus Cavernosum Dysfunction in Mice Fed a High Fat Diet. J Sex Med 2021;18(4):723–31.
[41] Li J, Huynh L, Cornwell WD, Tang M-S, Simborio H, Huang J, et al. Electronic Cigarettes Induce Mitochondrial DNA Damage and Trigger TLR9 (Toll-Like Receptor 9)-Mediated Atherosclerosis. Arterioscler Thromb Vasc Biol 2021;41 (2):839–53.
[42] Oka T, Hikoso S, Yamaguchi O, Taneike M, Takeda T, Tamai T, et al. Mitochondrial DNA that escapes from autophagy causes inflammation and heart failure. Nature 2012;485(7397):251–5.
[43] Yoshida K, Abe K, Ishikawa M, Saku K, Shinoda-Sakamoto M, Ishikawa T, et al. Inhibition of TLR9-NF-kappaB-mediated sterile inflammation improves pressure overload-induced right ventricular dysfunction in rats. Cardiovasc Res 2019;115(3):658–68.
[44] Xie L, He S, Kong N, Zhu Y, Tang Y, Li J, et al. Cpg-ODN, a TLR9 Agonist, Aggravates Myocardial Ischemia/Reperfusion Injury by Activation of TLR9-P38 MAPK Signaling. Cell Physiol Biochem 2018;47(4):1389–98.
[45] Dhondup Y, Sjaastad I, Sandanger Ø, Aronsen JM, Ahmed MS, Attramadal H, et al. Toll-Like Receptor 9 Promotes Survival in SERCA2a KO Heart Failure Mice. Mediators Inflamm 2017;2017:1–11.
[46] Guo Z, Tang N, Liu F-Y, Yang Z, Ma S-Q, An P, et al. TLR9 deficiency alleviates doxorubicin-induced cardiotoxicity via the regulation of autophagy. J Cell Mol Med 2020;24(18):10913–23.
[47] Tilstra JS, John S, Gordon RA, Leibler C, Kashgarian M, Bastacky S, et al. B cell-intrinsic TLR9 expression is protective in murine lupus. J Clin Invest 2020;130 (6):3172–87.
[48] Velten M, Duerr GD, Pessies T, Schild J, Lohner R, Mersmann J, et al. Priming with synthetic oligonucleotides attenuates pressure overload-induced inflammation and cardiac hypertrophy in mice. Cardiovasc Res 2012;96 (3):422–32.
[49] Nishimoto S, Fukuda D, Higashikuni Y, Tanaka K, Hirata Y, Murata C, et al. Obesity-induced DNA released from adipocytes stimulates chronic adipose tissue inflammation and insulin resistance. Sci Adv 2016;2(3):e1501332.
[50] Bugger H, Abel ED. Molecular mechanisms of diabetic cardiomyopathy. *Diabetologia* 2014;57(4):660–71.
[51] Veeranki S, Givvimani S, Kundu S, Metreveli N, Pushpakumar S, Tyagi SC. Moderate intensity exercise prevents diabetic cardiomyopathy associated contractile dysfunction through restoration of mitochondrial function and connexin 43 levels in db/db mice. J Mol Cell Cardiol 2016;92:163–73.

[52] Ding M, Feng N, Tang D, Feng J, Li Z, Jia M, et al. Melatonin prevents Drp1-mediated mitochondrial fission in diabetic hearts through SIRT1-PGC1α pathway. J Pineal Res 2018;65(2):e12491.
[53] Hu L, Ding M, Tang D, Gao E, Li C, Wang K, et al. Targeting mitochondrial dynamics by regulating Mfn2 for therapeutic intervention in diabetic cardiomyopathy. Theranostics 2019;9(13):3687–706.
[54] Lopaschuk GD, Ussher JR, Folmes CD, Jaswal JS, Stanley WC. Myocardial fatty acid metabolism in health and disease. Physiol Rev 2010;90(1):207–58.
[55] Alturki NA, McComb S, Ariana A, Rijal D, Korneluk RG, Sun S-C, et al. Triad3a induces the degradation of early necrosome to limit RipK1-dependent cytokine production and necroptosis. Cell Death Dis 2018;9(6).
[56] Schmitt H, Ulmschneider J, Billmeier U, Vieth M, Scarozza P, Sonnewald S, et al. The TLR9 Agonist Cobitolimod Induces IL10-Producing Wound Healing Macrophages and Regulatory T Cells in Ulcerative Colitis. J Crohns Colitis 2020;14(4):508–24.
[57] Schleimann MH, Kobberø M-L, Vibholm LK, Kjær K, Giron LB, Busman-Sahay K, et al. TLR9 agonist MGN1703 enhances B cell differentiation and function in lymph nodes. EBioMedicine 2019;45:328–40.
[58] Ribas A, Medina T, Kirkwood JM, Zakharia Y, Gonzalez R, Davar D, et al. Overcoming PD-1 Blockade Resistance with CpG-A Toll-Like Receptor 9 Agonist Vidutolimod in Patients with Metastatic Melanoma. Cancer Discov 2021;11(12):2998–3007.